



Citation for published version:

Fliegert, R, Bauche, A, Wolf Pérez, A-M, Watt, JM, Rozewitz, MD, Winzer, R, Janus, M, Gu, F, Rosche, A, Harneit, A, Flato, M, Moreau, C, Kirchberger, T, Wolters, V, Potter, BVL & Guse, AH 2017, '2-Deoxyadenosine 5-diphosphoribose is an endogenous TRPM2 superagonist', Nature Chemical Biology, vol. 13, pp. 1036-1044. <https://doi.org/10.1038/nchembio.2415>

DOI:

[10.1038/nchembio.2415](https://doi.org/10.1038/nchembio.2415)

Publication date:

2017

Document Version

Peer reviewed version

[Link to publication](#)

Publisher Rights

Unspecified

University of Bath

General rights

Copyright and moral rights for the publications made accessible in the public portal are retained by the authors and/or other copyright owners and it is a condition of accessing publications that users recognise and abide by the legal requirements associated with these rights.

Take down policy

If you believe that this document breaches copyright please contact us providing details, and we will remove access to the work immediately and investigate your claim.

1 **2'-Deoxyadenosine 5'-diphosphoribose is an endogenous TRPM2 superagonist**

2 Running Head: 2'-Deoxy-ADPR is an endogenous superagonist of TRPM2

3

4 Ralf Fliegert¹, Andreas Bauche¹, Adriana-Michelle Wolf Pérez¹, Joanna M. Watt^{2,3}, Monika
5 D. Rozewitz¹, Riekje Winzer¹, Mareike Janus¹, Feng Gu¹, Annette Rosche¹, Angelika
6 Harneit¹, Marianne Flato¹, Christelle Moreau², Tanja Kirchberger¹, Valerie Wolters¹, Barry
7 V.L. Potter^{2,3,*}, Andreas H. Guse^{1,*}

8 *equal contribution

9 ¹The Calcium Signalling Group, Department of Biochemistry and Molecular Cell Biology,
10 University Medical Centre Hamburg-Eppendorf, Martinistrasse 52, 20246 Hamburg,
11 Germany

12 ²Wolfson Laboratory of Medicinal Chemistry, Department of Pharmacy and Pharmacology,
13 University of Bath, Bath, BA2 7AY, UK

14 ³Medicinal Chemistry & Drug Discovery, Department of Pharmacology, University of
15 Oxford, Mansfield Road, Oxford, OX1 3QT, UK

16

17 **Abstract**

18 Transient receptor potential melastatin 2 (TRPM2), is a ligand-gated Ca²⁺-permeable non-
19 selective cation channel. While physiological stimuli, e.g. chemotactic agents, evoke
20 controlled Ca²⁺ signals via TRPM2, pathophysiological signals, such as reactive oxygen
21 species or genotoxic stress result in prolonged TRPM2-mediated Ca²⁺ entry and consequently
22 apoptosis. To date, adenosine 5'-diphosphoribose (ADPR, **1**) has been assumed to be the main
23 agonist for TRPM2. Here, we show that 2'-deoxy-ADPR **2** was a significantly better TRPM2

24 agonist, inducing 10.4-fold higher whole cell currents at saturation. Mechanistically, this
25 increased activity was caused by decreased rate of inactivation and higher average open
26 probability. Using high performance liquid chromatography (HPLC) and mass spectrometry,
27 endogenous 2'-deoxy-ADPR was detected in Jurkat T-lymphocytes. Consistently, cytosolic
28 nicotinamide mononucleotide adenylyltransferase 2 (NMNAT-2) and nicotinamide adenine
29 dinucleotide (NAD)-glycohydrolase CD38 sequentially catalyzed synthesis of 2'-deoxy-
30 ADPR from nicotinamide mononucleotide and 2'-deoxy-ATP *in vitro*. Thus, 2'-deoxy-ADPR
31 is an endogenous TRPM2 superagonist that may act as cell signaling molecule.

32

33 **Introduction**

34 The C-terminal domain of TRPM2 is homologous to ADPR pyrophosphatase NUDT9. This
35 discovery resulted in the identification of adenosine 5'-diphosphoribose (ADPR, **1**) as its
36 agonist¹. An increase in cellular ADPR to activate TRPM2 is thought to proceed by
37 hydrolysis of β -NAD either by NAD-glycohydrolase CD38 or via concerted action of poly-
38 ADPR polymerases (PARPs) and poly-ADPR glycohydrolase (PARG) (reviewed in ²). The
39 half maximal effective concentration (EC₅₀) for activation of TRPM2 by ADPR (reviewed in
40 ³) implies that a significant amount of cellular NAD must be converted to ADPR to achieve
41 activation. While this may make sense for the induction of apoptosis or cell death^{4,5}, it appears
42 rather unlikely to be the case for physiological activation of TRPM2, e.g. in chemotaxis⁶,
43 insulin secretion⁷, or thermosensation^{8,9}. Alternative activation mechanisms have been
44 described, including direct activation by hydrogen peroxide¹⁰, by intracellular Ca²⁺ ions¹¹ or
45 by *O*-acetyl-ADPR¹².

46 In summary, we show that among various ADPR analogues only 2'-deoxy-ADPR **2**, 3'-deoxy-
47 ADPR **17**, 2'-phospho-ADPR **15**, and 2-F-ADPR **13** activated TRPM2. 2'-Deoxy-ADPR **2**

48 activated TRPM2 with similar potency but higher efficacy than ADPR, making 2'-deoxy-
49 ADPR a TRPM2 superagonist. The massive increase in macroscopic current induced by 2'-
50 deoxy-ADPR was due to decelerated TRPM2 inactivation and a higher average open
51 probability, while the single channel conductance remained unaffected. Further, we
52 demonstrate formation of 2'-deoxy-ADPR *in vitro* in two steps: from NMN and 2'-deoxy-
53 ATP to 2'-deoxy-NAD as catalyzed by NMNAT-2, and from 2'-deoxy-NAD to 2'-deoxy-
54 ADPR catalyzed by CD38. Finally, we proved the presence of endogenous 2'-deoxy-ADPR
55 and 2'-deoxy-NAD and present evidence for hydrogen peroxide-evoked increase of 2'-deoxy-
56 ADPR in Jurkat T cells. Importantly, 2'-deoxy-ADPR is not only a significantly better agonist
57 regarding TRPM2 activation than ADPR, but in addition does not require any NAD
58 consumption for its synthesis. 2'-deoxy-ADPR thus exhibits many of the properties expected
59 of a second messenger.

60

61 **Results**

62 *2'-Deoxy-ADPR as a TRPM2 superagonist*

63 Our interest in 2'-deoxy-ADPR as a potential TRPM2 agonist began when we probed the
64 structural requirements for activation of the channel. We assessed the agonist activity of
65 ADPR analogues (Supplementary Results, Supplementary Fig. 1–4) we had previously
66 evaluated as potential TRPM2 inhibitors¹³. These analogues feature modifications in the
67 purine base, the adenosine ribose, the pyrophosphate group and the terminal ribose. Published
68 EC₅₀ values for the activation of TRPM2 by ADPR are in the micromolar range (between
69 1 μmol/L and 90 μmol/L)³ indicating an interaction of rather low affinity. We therefore
70 anticipated that many of the analogues might activate TRPM2. To our surprise most of the
71 analogues had no, or negligible, agonist activity (Fig. 1). Among the ADPR analogues with

72 modifications at the purine ring only 2-F-ADPR retained partial agonist activity (Fig. 1).
73 These results clearly demonstrate the requirement of a combination of terminal ribose,
74 pyrophosphate, and adenosine motifs for activation of TRPM2.

75 The part of ADPR most permissive to modifications was the adenosine ribose (Fig. 2). 2'-
76 Phospho-ADPR showed partial agonist activity albeit at higher concentrations (EC_{50}
77 $110 \mu\text{mol/L}$) and with reduced efficacy ($0.56 \text{ nA} \pm 0.64 \text{ nA}$, best-fit value \pm standard error
78 (SE)) compared to ADPR ($1.60 \text{ nA} \pm 0.47 \text{ nA}$, best-fit value \pm SE) (Fig. 2a), in good
79 agreement with a recent study¹⁴. The most interesting finding, however, came from our
80 attempt to establish the role of the 2'- and 3'-hydroxyl groups of the adenosine ribose. While
81 3'-deoxy-ADPR showed an EC_{50} comparable to that of ADPR (EC_{50} $46 \mu\text{mol/L}$ and
82 $28 \mu\text{mol/L}$, respectively) and elicited only a slightly reduced maximum current ($1.23 \text{ nA} \pm$
83 0.52 nA , best-fit value \pm SE), 2'-deoxy-ADPR activated TRPM2 at somewhat lower
84 concentrations than ADPR (Fig. 2a). Most importantly, 2'-deoxy-ADPR induced 10.4-fold
85 higher currents in the whole cell configuration (Fig. 2a). Whole cell patch clamp experiments
86 with the human T cell line Jurkat that endogenously expresses TRPM2^{4,15-17} confirmed the
87 induction of significantly higher currents by 2'-deoxy-ADPR as compared to ADPR. In
88 contrast to HEK293 cells, Jurkat cells in the majority of experiments did not tolerate 2'-
89 deoxy-ADPR concentrations $> 100 \mu\text{mol/L}$, likely due to the high Ca^{2+} and Na^{+} influx (Fig.
90 2b). Under physiological ionic conditions, in these experiments the I-V curve obtained from
91 voltage ramps was nearly linear and was characterized by a reversal potential near 0
92 (Supplementary Fig. 5b), regardless of the activating agonist. These results clearly
93 demonstrate that 2'-deoxy-ADPR is a TRPM2 superagonist.

94 The increase in whole cell current after activation by superagonists might be explained either
95 by the preferential occupation of higher conductance states, as has been shown for the
96 insecticide clothianidin, a superagonist of the nicotinic acetylcholine receptor¹⁸, by induction

97 of an otherwise inaccessible higher conductance state, or by a change in kinetics allowing the
98 channel to remain in the open state for longer periods of time, as is the case for 4,5,6,7-
99 tetrahydroisoxazolo[5,4-*c*]pyridin-3(2*H*)-one (THIP), a superagonist of the $\alpha_4\beta_3\delta$ GABA
100 receptor¹⁹. To distinguish between these possibilities we performed recordings on excised
101 inside/out patches from cells expressing either wild type hTRPM2 (Fig 3a+b+c) or hTRPM2
102 with modified selectivity filter (T5L) that shows increased affinity to permeating cations
103 resulting in higher single channel conductivity²⁰. The results showed no significant difference
104 in single channel conductance (Fig. 3c) upon activation by either ADPR or 2'-deoxy-ADPR.
105 Instead, the inactivation of TRPM2 following 2'-deoxy-ADPR activation was significantly
106 slower compared to ADPR (Fig 3d+e+f; 2'-deoxy ADPR: $0.050 \text{ s}^{-1} \pm 0.003 \text{ s}^{-1}$ vs ADPR:
107 $0.037 \text{ s}^{-1} \pm 0.003 \text{ s}^{-1}$, best-fit values \pm SE, extra sum-of-squares F test, $p=0.001$). Further, the
108 average open probability was 37% higher (Fig. 3d+g) for activation by 2'-deoxy-ADPR
109 (median 0.92, interquartile range (IQR) 0.80 to 0.97) compared to ADPR (median 0.67, IQR
110 0.17 to 0.74, Mann-Whitney test, $p<0.0001$). In addition, we also observed an approx. 5-fold
111 increase in the number of channels simultaneously in the open state when excised patches
112 were exposed to 2'-deoxy-ADPR (Fig. 3d+h), at least partially attributable to the increased
113 open probability. Whole cell patch clamp experiments with different Ca^{2+} concentrations in
114 the pipette buffer solution demonstrated a reduced Ca^{2+} -sensitivity of activation of TRPM2 by
115 2'-deoxy-ADPR when compared to activation by ADPR (Fig. 2c). Whereas the maximum
116 current induced by ADPR (as obtained from the concentration-response curve) increased by
117 140% (from $0.67 \text{ nA} \pm 1.07 \text{ nA}$ to $1.60 \text{ nA} \pm 0.47 \text{ nA}$) when the free $[\text{Ca}^{2+}]$ was raised from
118 50 nmol/L to 200 nmol/L, the maximum current induced by 2'-deoxy-ADPR increased only
119 by 16% (from $14.3 \text{ nA} \pm 1.45 \text{ nA}$ to $16.7 \text{ nA} \pm 0.74 \text{ nA}$, best-fit values \pm SE). At
120 (supraphysiological) saturating concentrations for Ca^{2+} and ADPR the open probability of
121 human TRPM2 approaches a value of one²¹. It therefore seems likely that in intact cells

122 activation by 2'-deoxy-ADPR is less sensitive to Ca^{2+} , with the concentration-response for
123 Ca^{2+} shifted to the left, allowing for higher open probabilities and larger whole cell currents at
124 physiological Ca^{2+} concentrations.

125 *Biosynthetic pathways for 2'-deoxy-ADPR*

126 Superagonist behavior has previously been observed with pharmacological modulators of
127 ligand-gated ion channels usually having little or no resemblance to the natural ligands.
128 However, 2'-deoxy-ADPR is closely related to ADPR. Thus, we hypothesized that 2'-deoxy-
129 ADPR might be an endogenous modulator of TRPM2.

130 A conceivable endogenous pathway to 2'-deoxy-ADPR would be the hydrolysis of 2'-deoxy-
131 NAD by either CD38 or the PARP/PARG system. 2'-Deoxy-NAD can be synthesized by
132 nicotinamide mononucleotide adenylyltransferase (NMNAT, EC 2.7.7.1) catalyzing the
133 condensation of β -nicotinamide mononucleotide (NMN) and 2'-deoxy-ATP, as has been
134 shown for NMNAT from yeast²² and human NMNAT-1²³. There are three different isoforms
135 of NMNAT with distinct subcellular localization that contribute to different NAD pools²⁴.
136 Here we demonstrate for the first time that NMNAT-2, the isoform that presumably maintains
137 the cytoplasmic NAD pool²⁴, also catalyzed the conversion of 2'-deoxy-ATP and NMN to 2'-
138 deoxy-NAD (Fig. 4a; Supplementary Fig. 6). At a saturating concentration of 500 $\mu\text{mol/L}$ β -
139 NMN the $K_{0.5}$ for 2'-deoxy-ATP is 3.28 mmol/L \pm 0.55 mmol/L (Michaelis-Menten constant
140 K_M for ATP 611 $\mu\text{mol/L}$ \pm 31 $\mu\text{mol/L}$, both best-fit values \pm SE). Interestingly, the enzyme
141 did not only show cooperativity (Hill coefficient n_H 1.4 \pm 0.1, best-fit value \pm SE) with regard
142 to 2'-deoxy ATP, but was also inhibited by high concentrations of the substrate, which is
143 clearly not the case for ATP (Fig. 4b).

144 Next we explored potential pathways for generation of 2'-deoxy-ADPR via both the
145 PARP/PARG and CD38 pathways. Since it was shown in isolated nuclei that 2'-deoxy-ADPR

146 was incorporated into poly-ADPR polymers of nuclear proteins²⁵, we analyzed whether poly-
147 ADP ribosylated proteins actually contain 2'-deoxy-ADPR residues. Poly-ADP-ribosylated
148 proteins were isolated from HEK293 cells previously exposed to H₂O₂^{5,26}. An increase of the
149 amount of poly-ADP ribosylated proteins, compared to unstimulated controls was confirmed
150 by western blot analysis (Supplementary Fig. 7, upper inset). The immunoprecipitate was then
151 hydrolyzed by recombinant human PARG. Analysis of products by HPLC showed significant
152 amounts of ADPR and a small amount of AMP, most likely due to spontaneous degradation
153 of ADPR (Supplementary Fig. 7, central panel), but despite the high sensitivity of the method
154 (40 fmol at signal-to-noise (S/N) ratio ≥ 3) no 2'-deoxy-ADPR was detected (Supplementary
155 Fig. 7, central and lower panel). Thus, it is unlikely that release of 2'-deoxy-ADPR from poly-
156 ADP-ribosylated proteins by PARG significantly contributes to TRPM2 activation.

157 Next we tested whether CD38 might produce 2'-deoxy-ADPR. CD38 is well known to be
158 expressed as ecto-enzyme (type II orientation), but recently evidence for type III orientation
159 with the active site facing the cytoplasm was presented²⁷, thereby potentially allowing
160 turnover of cytosolic 2'-deoxy-NAD. Recombinant soluble human CD38 completely
161 hydrolyzed 2'-deoxy-NAD to a product that co-eluted with chemically synthesized 2'-deoxy-
162 ADPR (Fig. 4c). Product identity was confirmed by spiking with authentic 2'-deoxy-ADPR
163 (Supplementary Fig. 8a) and hydrolysis by pyrophosphatase to 2'-deoxy-AMP
164 (Supplementary Fig. 8b). Further, type III CD38 enzyme activity, though small in comparison
165 to ecto-enzyme (type II) CD38 enzyme activity, was clearly detected in Jurkat T cells (Fig
166 4d). While in CD38^{-/-} cells measurable NAD glycohydrolase was not detected (Fig. 4d, left),
167 specific inhibition of ecto-CD38 by 2'-deoxy-2'-fluoro arabinosyl NAD (araF-NAD)²⁸,
168 forming a stable covalent inhibitor-CD38 complex, almost completely abolished type II CD38
169 activity (Fig. 4d, middle, 1st araF-NAD addition). Permeabilization of such cells with saponin
170 allowed to access type III CD38 and to determine its activity (Fig. 4d, right). Specificity was

171 demonstrated by a 2nd addition of araF-NAD fully blocking type III CD38 (Fig. 4d, right).
172 Kinetic analysis using NAD vs 2'-deoxy-NAD as substrates resulted in 9.2-fold higher affinity
173 of CD38 for 2'-deoxy-NAD and comparable values for maximal velocity V_{\max}
174 (Supplementary Fig. 8c). Collectively, strong evidence is presented that 2'-deoxy-NAD serves
175 as a substrate for type III CD38 to produce 2'-deoxy-ADPR, while 2'-deoxy-NAD can be
176 produced from the abundant cellular metabolites nicotinamide mononucleotide and 2'-deoxy-
177 ATP by cytosolic NMNAT (Supplementary Fig. 9).

178 *2'-Deoxy-ADPR and 2'-deoxy-NAD present in Jurkat cells*

179 To detect endogenous 2'-deoxy-ADPR and 2'-deoxy-NAD in Jurkat T cells, we used two
180 consecutive reversed phase (RP)-HPLC separations on C8 and C18 columns using a volatile
181 ammonium acetate buffer to allow for subsequent high resolution mass spectrometry (Fig. 5).
182 Fractions pre-fractionated on a C8 column (Fig. 5a) and co-eluting with 2'-deoxy-ADPR and
183 2'-deoxy-NAD on a C18 column (Fig. 5b+c) showed molecular ions corresponding to 2'-
184 deoxy-ADPR (observed mass $[M-H]^-$ 542.0722, calculated mass: 542.0695) and 2'-deoxy-
185 NAD (observed mass $[M-H]^-$ 646.1104, calculated mass: 646.1069) (Supplementary Fig. 10
186 a+b). The main electrospray ionization (ESI) fragmentation products of 2'-deoxy-ADPR and
187 2'-deoxy-NAD, 2'-deoxy-AMP ($[M-H]^-$ 330.0633) and 2'-deoxy-ADP ($[M-H]^-$ 410.0304),
188 were prominent in both samples. Since it is unlikely that both products co-eluted with 2'-
189 deoxy-ADPR and 2'-deoxy-NAD during two-dimensional HPLC, these molecular ions are
190 most likely to result from fragmentation of 2'-deoxy-ADPR and 2'-deoxy-NAD during mass
191 spectrometry. The HPLC system based on ammonium acetate eluents was suitable for
192 quantification of endogenous 2'-deoxy-NAD (Fig. 5c+g), amounting to 5.05 ± 0.58
193 pmol/ 10^7 cells (mean \pm SEM, n=12, significantly different from a theoretical median of 0,
194 Wilcoxon Signed Rank Test). The concentration of 2'-deoxy-NAD was not significantly
195 affected by exposure of the cells to hydrogen peroxide (5.67 ± 0.78 pmol/ 10^7 cells, mean \pm

196 SEM, n=11) (Fig. 5c+g). To investigate any role of CD38 in the synthesis of 2'-deoxy-ADPR
197 in Jurkat T cells, CD38 was knocked-out using CRISPR (Clustered Regularly Interspaced
198 Short Palindromic Repeats)/Cas9 technology^{29,30}. P10 membranes of the resulting CD38^{-/-} cell
199 line did not show NAD glycohydrolase activity and were negative for CD38 in western blot
200 analysis (Supplementary Fig 11). Neither was the endogenous concentration of 2'-deoxy-
201 NAD significantly affected by knock-out of CD38 nor by hydrogen peroxide stimulation (Fig.
202 5 d+f+g). In addition, we also analyzed cellular ADPR and NAD contents under these
203 conditions (Supplementary Fig 12). As expected, NAD was present in much higher quantities
204 (7.58 ± 0.42 nmol/10⁷ cells, mean±SEM, n=12), but was not affected by knockout of NAD
205 glycohydrolase CD38 (6.42 ± 0.30 nmol/10⁷ cells, mean±SEM, n=15). Exposure to hydrogen
206 peroxide did, at least during the 5 min of the experiment, not affect NAD (p=0.78 for wild
207 type and p=0.62 for CD38^{-/-} cells). ADPR was found in quantities (292 ± 79 pmol/10⁷ cells,
208 mean±SEM, n=11) consistent with our previous results⁴, but was neither significantly affected
209 by knockout of CD38 nor by exposure to hydrogen peroxide.

210 In contrast to almost baseline-separated 2'-deoxy-NAD (Fig. 5c+f), HPLC using volatile
211 ammonium acetate buffer (ideally suited for subsequent mass spectrometry) did not allow for
212 baseline separation of 2'-deoxy-ADPR (Fig. 5b+e). Though 2'-deoxy-ADPR was qualitatively
213 identified (i) by its retention time, (ii) by using samples from cell extracts spiked with a small
214 amount of authentic 2'-deoxy-ADPR (Fig. 5b+e), and (iii) by mass spectrometry
215 (Supplementary Fig. 10a), the separation on a C18 column was not sufficient to quantify 2'-
216 deoxy-ADPR reliably (Fig. 5b+e). However, we noted that the peak containing 2'-deoxy-
217 ADPR increased after stimulation with hydrogen peroxide. Further, comparison of the
218 chromatograms of samples from wildtype (Fig. 5b) and CD38^{-/-} cells (Fig. 5e) shows that the
219 peak containing 2'-deoxy-ADPR was absent in the samples from CD38^{-/-} cells regardless of

220 whether they have been exposed to H₂O₂ or not, suggesting that 2'-deoxy-ADPR is produced
221 from 2'-deoxy-NAD by CD38.

222 Using ion-pair instead of conventional RP-HPLC, two consecutive separations on C8 and C18
223 columns (Fig. 6) resulted in sufficient separation of endogenous 2'-deoxy-ADPR for
224 quantification (Fig. 6a, lower panel). Here, 2'-deoxy-ADPR was identified using authentic 2'-
225 deoxy-ADPR as standard or in a spiked sample (Fig 6a). Recovery of 2'-deoxy-ADPR was
226 determined using 1, N⁶-etheno-adenosine (Supplementary Fig 13). Any trials to identify 2'-
227 deoxy-ADPR by mass spectrometry in this HPLC system failed due to the presence of the ion
228 pair reagent in the collected samples; furthermore, several procedures tested to deplete the ion
229 pair reagent were not successful. However, using this ion-pair RP-HPLC separations on C8
230 and C18 columns, 2'-deoxy-ADPR was detected in Jurkat cells and determined to be
231 35 pmol/10⁷ cells (median, interquartile range (IQR): 17 pmol/10⁷ cells to 50 pmol/10⁷ cells,
232 significantly different from a theoretical median of 0, Wilcoxon Signed Rank Test). As
233 hydrogen peroxide treatment results in TRPM2 activation, we then tested the impact of H₂O₂
234 on the endogenous 2'-deoxy-ADPR concentration (Fig. 6b+c). After 5 min the amount of 2'-
235 deoxy-ADPR rose significantly by 2.71 fold to 95 pmol/10⁷ cells (median, IQR: 42
236 pmol/10⁷ cells to 116 pmol/10⁷ cells).

237 **Discussion**

238 It is widely accepted that TRPM2 can be activated downstream of reactive oxygen species
239 like hydrogen peroxide^{10,31}. Despite reports of direct activation of the channel by hydrogen
240 peroxide³², this has mostly been attributed to the generation of ADPR by the consecutive
241 action of PARP and PARG^{5,33}. Especially during certain cell cycle phases, 2'-deoxy-ADPR as
242 an additional mechanism might contribute to this process: hydrogen peroxide-induced DNA
243 damage can cause a replication arrest during S phase, which would result in an accumulation

244 of 2'-deoxy-ATP, because deoxy-nucleoside triphosphates will no longer be consumed by the
245 replication machinery. In addition, the activation of PARPs following DNA damage will
246 result in consumption of NAD for poly-ADP ribosylation. The consequent drop in cellular
247 NAD will increase its synthesis, which ultimately results in decreased cellular ATP pools. The
248 increased ratio of 2'-deoxy-ATP to ATP then facilitates synthesis of 2'-deoxy-NAD by
249 NMNAT and subsequent hydrolysis to 2'-deoxy-ADPR by CD38. The latter reaction is
250 preferred due to the 9.2-fold higher affinity of CD38 for 2'-deoxy-NAD, as compared to NAD
251 (see Supplementary Fig. 8c). The increase in cellular 2'-deoxy-ADPR then either mediates
252 TRPM2 activation on its own or contributes to TRPM2 activation mediated by ADPR derived
253 from PARP/PARG activity.

254 How do the nucleotide determinations from cell extracts translate into cytosolic, or even sub-
255 plasmalemmal, concentrations? Assuming a mean diameter of Jurkat cells of $11.5 \mu\text{m}^3$, a
256 cellular 2'-deoxy-ADPR concentration of $4.4 \mu\text{mol/L}$ can be calculated. However, the
257 lymphocyte is not simply a sphere filled with aqueous liquid, but contains solid material, e.g.
258 organelles, DNA, proteins. This solid portion is difficult to calculate, but well known for
259 Jurkat cells is the nucleus volume, amounting to 55% of the total volume³⁴. Using this portion
260 to distinguish the cytosolic from the intra-nuclear space, the cytosolic concentration of 2'-
261 deoxy-ADPR amounts to $9.8 \mu\text{mol/L}$, a value found in the lower part of the concentration-
262 response curve (Fig. 2). Upon stimulation by hydrogen peroxide this cytosolic concentration
263 within 5 min rises to $26.6 \mu\text{mol/L}$. If we further assume that the concentration of 2'-deoxy-
264 ADPR in the cytosol is not evenly distributed, but is increased at the site of its biosynthesis,
265 the sub-plasmalemmal space where the catalytic center of type III CD38 is localized²⁷, then
266 the local concentrations are readily in the dynamic range of the concentrations response
267 curve(s) shown in Fig. 2, especially at slightly elevated free cytosolic Ca^{2+} concentrations,
268 e.g. 200 nM (Fig. 2c). Besides 2'-deoxy-ADPR, we also established the presence of

269 endogenous 2'-deoxy-NAD, the potential precursor of 2'-deoxy-ADPR. The cytosolic
270 concentration of 2'-deoxy-NAD is low at 1.41 $\mu\text{mol/L}$, in comparison to the cellular
271 concentration of NAD (955 $\mu\text{mol/L}$). This indicates that 2'-deoxy-NAD represents a
272 nucleotide with specialized function(s), very much in contrast to NAD that serves as (co)-
273 substrate for a plethora of enzymatic reactions. The kinetic parameters obtained for NMNAT-
274 2 (Fig. 2c) suggest that inside the cell mainly ATP is used to maintain the cellular NAD pool.
275 However, upon stimulation with hydrogen peroxide, small amounts of 2'-deoxy-ATP appear
276 to flux via 2'-deoxy-NAD into 2'-deoxy-ADPR; substrate inhibition of NMNAT-2 by 2'-
277 deoxy-ATP, but not ATP, indicates that the pathway towards 2'-deoxy-ADPR is a highly
278 regulated process. It has not escaped our notice that the presence of endogenous 2'-deoxy-
279 NAD also in principle presents the possibility for generation of 2'-deoxy-cADPR by CD38, in
280 addition to 2'-deoxy ADPR. While 2'-deoxy-cADPR was shown to be equipotent to cADPR
281 in Ca^{2+} signaling in sea urchin³⁵, like its 3'-deoxy congener, it was not active in Jurkat T
282 cells³⁶ excluding the need to consider 2'-deoxy-cADPR more widely in a signaling context.

283 Our results might solve an important conceptual problem concerning activation of TRPM2:
284 Cellular NAD serves many functions, most prominently as redox coenzyme, as co-substrate
285 for sirtuins, and as precursor for nicotinamide adenine dinucleotide phosphate (NADP) and
286 the second messengers cyclic adenosine diphosphoribose (cADPR) and nicotinic acid adenine
287 dinucleotide phosphate (NAADP, reviewed in²⁴). NAD depletion appears therefore
288 incompatible with life and has been shown to ultimately result in cell death³⁷. We therefore
289 consider it unlikely that during physiological activation the amount of ADPR necessary for
290 TRPM2 activation, especially at resting Ca^{2+} concentrations, is generated by turnover of
291 nuclear, cytosolic or mitochondrial NAD pools. In contrast, a small cytosolic pool of 2'-
292 deoxy-NAD might be maintained, for instance by NMNAT, independently of NAD, since 2'-
293 deoxy-NAD can neither be phosphorylated by NAD kinase to yield 2'-deoxy-NADP nor is it a

294 good substrate for NAD dependent dehydrogenases^{22,38,39}. Thus, formation of 2'-deoxy-ADPR
295 from 2'-deoxy-NAD by type III CD38 does not interfere with energy metabolism and other
296 NAD functions. Previous work demonstrating that CD38 hydrolyzed 2'-deoxy-NAD with
297 similar V_{\max} as NAD⁴⁰ is confirmed here; however, a 9.2-fold higher affinity for 2'-deoxy-
298 NAD as compared to NAD was determined (Supplementary Fig. 8c). Thus, we present here a
299 possible mechanism for the generation of 2'-deoxy-ADPR via conversion of cytosolic 2'-
300 deoxy-NAD by CD38 in a type III orientation. However, since the endogenous concentration
301 of 2'-deoxy-NAD is small and the relative activity of CD38 in the type III orientation that we
302 observed was low, generation of 2'-deoxy-ADPR may be accomplished via alternative
303 pathways.

304 Taken together, we demonstrate that 2'-deoxy-ADPR is the most efficient endogenous agonist
305 of TRPM2 described to date. In addition, 2'-deoxy-ADPR appears to be the first superagonist
306 for an ion channel that can be synthesized by the enzymatic machinery of most cell types. Our
307 results suggest the possibility that TRPM2 can be activated in context-specific manner. In
308 pathological cell death in neurodegenerative diseases⁴¹, stroke⁴², or myocardial infarction⁴³,
309 ADPR may be generated by PARP/PARG³³ or by CD38 thereby not only triggering TRPM2
310 activation, but also depleting cellular NAD and ATP pools. In contrast, since physiological
311 processes, e.g. neutrophil chemotaxis, require an intact cytoplasmic NAD pool, 2'-deoxy-
312 ADPR may activate TRPM2 without consumption of NAD, thus acting independently of
313 energy metabolism. Taken together, the confluence of properties associated with 2'-deoxy-
314 ADPR may point to a physiological role for the molecule as a novel second messenger
315 activating TRPM2.

316

317 **Acknowledgements**

318 This study was supported by the Deutsche Forschungsgemeinschaft (GU 360/16-1 to AHG),
319 the Wellcome Trust (Project Grant 084068 to BVLP and AHG and Programme Grant 082837
320 to BVLP), and Landesforschungsförderung Hamburg (Research Group ReAd Me to AHG).
321 BVLP is a Wellcome Trust Senior Investigator (Grant 101010).

322

323

324 **Author contributions**

325 AHG, BVLP and RF designed the study and individual experiments. CM and JMW
326 synthesized and purified the ADPR analogues. TK, RF and MDR performed
327 electrophysiological characterization of ADPR analogues. MDR carried out the single channel
328 recordings. AMWP and AB performed the enzyme assays with NMNAT and CD38. RW
329 analyzed nucleotide products from poly ADP-ribosylated proteins. RF and AH prepared
330 TRPM2 T5L and CD38 expression vectors and generated the TRPM2 T5L cell line. AB,
331 AWMP and MJ established the HPLC method for determination of endogenous 2'-deoxy-
332 ADPR. AB and MJ quantitatively analyzed endogenous nucleotides. AB determined substrate
333 saturation plots for NMNAT-2 and sCD38. JMW performed the HRMS analysis of 2'-deoxy-
334 ADPR and 2'-deoxy-NAD. VW generated the CD38^{-/-} Jurkat cell line and produced and
335 purified soluble recombinant CD38. MF characterized the CD38^{-/-} Jurkat cell line. AR, AB
336 and FG determined the activity of CD38 in type III orientation. All authors wrote the
337 manuscript.

338

339 **References for main text**

340 1. Perraud, A. L. *et al.* ADP-ribose gating of the calcium-permeable LTRPC2 channel

- 341 revealed by Nudix motif homology. *Nature* **411**, 595–599 (2001).
- 342 2. Knowles, H., Li, Y. & Perraud, A. L. The TRPM2 ion channel, an oxidative stress and
343 metabolic sensor regulating innate immunity and inflammation. *Immunol. Res.* **55**,
344 241–248 (2013).
- 345 3. Faouzi, M. & Penner, R. in *Mammalian Transient Receptor Potential (TRP) Cation*
346 *Channels* (eds. Dietrich, A. & Gudermann, T.) **222**, 157–188 (2014).
- 347 4. Gasser, A. *et al.* Activation of T cell calcium influx by the second messenger ADP-
348 ribose. *J. Biol. Chem.* **281**, 2489–2496 (2006).
- 349 5. Buelow, B., Song, Y. & Scharenberg, A. M. The Poly(ADP-ribose) polymerase PARP-
350 1 is required for oxidative stress-induced TRPM2 activation in lymphocytes. *J. Biol.*
351 *Chem.* **283**, 24571–24583 (2008).
- 352 6. Partida-Sanchez, S. *et al.* Chemotaxis of mouse bone marrow neutrophils and dendritic
353 cells is controlled by adp-ribose, the major product generated by the CD38 enzyme
354 reaction. *J. Immunol.* **179**, 7827–7839 (2007).
- 355 7. Uchida, K. *et al.* Lack of TRPM2 impaired insulin secretion and glucose metabolisms
356 in mice. *Diabetes* **60**, 119–126 (2011).
- 357 8. Song, K. *et al.* The TRPM2 channel is a hypothalamic heat sensor that limits fever and
358 can drive hypothermia. *Science* **353**, 1393–1398 (2016).
- 359 9. Tan, C.-H. & McNaughton, P. A. The TRPM2 ion channel is required for sensitivity to
360 warmth. *Nature* **536**, 460–3 (2016).
- 361 10. Wehage, E. *et al.* Activation of the cation channel long transient receptor potential
362 channel 2 (LTRPC2) by hydrogen peroxide: A splice variant reveals a mode of
363 activation independent of ADP-ribose. *J. Biol. Chem.* **277**, 23150–23156 (2002).

- 364 11. Du, J., Xie, J. & Yue, L. Intracellular calcium activates TRPM2 and its alternative
365 spliced isoforms. *Proc. Natl. Acad. Sci. U. S. A.* **106**, 7239–7244 (2009).
- 366 12. Grubisha, O. *et al.* Metabolite of SIR2 reaction modulates TRPM2 ion channel. *J. Biol.*
367 *Chem.* **281**, 14057–14065 (2006).
- 368 13. Moreau, C. *et al.* Structure-activity relationship of adenosine 5'-diphosphoribose at the
369 transient receptor potential melastatin 2 (TRPM2) channel: Rational design of
370 antagonists. *J. Med. Chem.* **56**, 10079–10102 (2013).
- 371 14. Tóth, B., Iordanov, I. & Csanády, L. Ruling out pyridine dinucleotides as true TRPM2
372 channel activators reveals novel direct agonist ADP-ribose-2'-phosphate. *J. Gen.*
373 *Physiol.* **145**, 419–430 (2015).
- 374 15. Sano, Y. *et al.* Immunocyte Ca²⁺ influx system mediated by LTRPC2. *Science* **293**,
375 1327–1330 (2001).
- 376 16. Beck, A., Kolisek, M., Bagley, L. A., Fleig, A. & Penner, R. Nicotinic acid adenine
377 dinucleotide phosphate and cyclic ADP-ribose regulate TRPM2 channels in T
378 lymphocytes. *FASEB J.* **20**, 962–4 (2006).
- 379 17. Klumpp, D. *et al.* Targeting TRPM2 Channels Impairs Radiation-Induced Cell Cycle
380 Arrest and Fosters Cell Death of T Cell Leukemia Cells in a Bcl-2-Dependent Manner.
381 *Oxid. Med. Cell. Longev.* **2016**, 8026702 (2016).
- 382 18. Brown, L. A., Ihara, M., Buckingham, S. D., Matsuda, K. & Sattelle, D. B.
383 Neonicotinoid insecticides display partial and super agonist actions on native insect
384 nicotinic acetylcholine receptors. *J. Neurochem.* **99**, 608–615 (2006).
- 385 19. Mortensen, M., Ebert, B., Wafford, K. & Smart, T. G. Distinct activities of GABA
386 agonists at synaptic- and extrasynaptic-type GABA_A receptors. *J. Physiol.* **588**, 1251–

- 387 1268 (2010).
- 388 20. Tóth, B. & Csanády, L. Pore collapse underlies irreversible inactivation of TRPM2
389 cation channel currents. *Proc. Natl. Acad. Sci. U. S. A.* **109**, 13440–13445 (2012).
- 390 21. Csanády, L. & Töröcsik, B. Four Ca²⁺ ions activate TRPM2 channels by binding in
391 deep crevices near the pore but intracellularly of the gate. *J. Gen. Physiol.* **133**, 189–
392 203 (2009).
- 393 22. Klenow, H. & Andersen, B. Some enzyme reactions with adenine deoxyriboside
394 polyphosphates. *Biochim. Biophys. Acta* **23**, 92–97 (1957).
- 395 23. Emanuelli, M. *et al.* Molecular cloning, chromosomal localization, tissue mRNA
396 levels, bacterial expression, and enzymatic properties of human NMN
397 adenylyltransferase. *J. Biol. Chem.* **276**, 406–412 (2001).
- 398 24. Di Stefano, M. & Conforti, L. Diversification of NAD biological role: the importance
399 of location. *FEBS J.* **280**, 4711–28 (2013).
- 400 25. Suhadolnik, R. J. *et al.* ADP-Ribosylation of Isolated Nuclei from HeLa Cells, Rat
401 Liver , Fetal Rat Liver , and Novikoff Rat Hepatoma. *J. Biol. Chem.* **252**, 4134–4144
402 (1977).
- 403 26. Bakondi, E. *et al.* Detection of poly(ADP-ribose) polymerase activation in oxidatively
404 stressed cells and tissues using biotinylated NAD substrate. *J. Histochem. Cytochem.*
405 **50**, 91–8 (2002).
- 406 27. Zhao, Y. J., Lam, C. M. C. & Lee, H. C. The Membrane-Bound Enzyme CD38 Exists
407 in Two Opposing Orientations. *Sci. Signal.* **5**, ra67-ra67 (2012).
- 408 28. Muller-Steffner, H. M., Malver, O., Hosie, L., Oppenheimer, N. J. & Schuber, F. Slow-
409 binding inhibition of NAD⁺ glycohydrolase by arabino analogues of beta-NAD. *J.*

- 410 *Biol. Chem.* **267**, 9606–11 (1992).
- 411 29. Mali, P. *et al.* RNA-guided human genome engineering via Cas9. *Science* **339**, 823–6
412 (2013).
- 413 30. Cong, L. *et al.* Multiplex genome engineering using CRISPR/Cas systems. *Science*
414 **339**, 819–23 (2013).
- 415 31. Hara, Y. *et al.* LTRPC2 Ca²⁺-permeable channel activated by changes in redox status
416 confers susceptibility to cell death. *Mol. Cell* **9**, 163–73 (2002).
- 417 32. Heiner, I. *et al.* Expression profile of the transient receptor potential (TRP) family in
418 neutrophil granulocytes: evidence for currents through long TRP channel 2 induced by
419 ADP-ribose and NAD. *Biochem. J.* **371**, 1045–53 (2003).
- 420 33. Fonfria, E. *et al.* TRPM2 channel opening in response to oxidative stress is dependent
421 on activation of poly(ADP-ribose) polymerase. *Br. J. Pharmacol.* **143**, 186–192
422 (2004).
- 423 34. Rosenbluth, M. J., Lam, W. A. & Fletcher, D. A. Force microscopy of nonadherent
424 cells: a comparison of leukemia cell deformability. *Biophys. J.* **90**, 2994–3003 (2006).
- 425 35. Ashamu, G. A., Sethi, J. K., Galione, A. & Potter, B. V. Roles for adenosine ribose
426 hydroxyl groups in cyclic adenosine 5'-diphosphate ribose-mediated Ca²⁺ release.
427 *Biochemistry* **36**, 9509–17 (1997).
- 428 36. Moreau, C. *et al.* Synthesis of cyclic adenosine 5'-diphosphate ribose analogues: a
429 C2'endo/syn 'southern' ribose conformation underlies activity at the sea urchin cADPR
430 receptor. *Org. Biomol. Chem.* **9**, 278–90 (2011).
- 431 37. Del Nagro, C., Xiao, Y., Rangell, L., Reichelt, M. & O'Brien, T. Depletion of the
432 Central Metabolite NAD Leads to Oncosis-mediated Cell Death. *J. Biol. Chem.* **289**,

- 433 35182–92 (2014).
- 434 38. Dahmen, W., Webb, B. & Preiss, J. The Deamido-Diphosphopyridine Nucleotide and
435 Diphosphopyridine Nucleotide Pyrophosphorylases of *Escherichia coli* and Yeast.
436 *Arch. Biochem. Biophys.* **120**, 440–450 (1967).
- 437 39. Suhadolnik, R. J., Lennon, M. B., Uematsu, T., Monahan, J. E. & Baur, R. Role of
438 adenine ring and adenine ribose of NAD⁺ in binding and catalysis with alcohol
439 dehydrogenase, lactic dehydrogenase and glyceraldehyde-3-phosphate dehydrogenase.
440 *J. Biol. Chem.* **252**, 4125–4133 (1977).
- 441 40. Schuber, F., Pascal, M. & Travo, P. Calf Spleen Nicotinamide Adenine Dinucleotide
442 Glycohydrolase. Properties of the Active Site. *Eur. J. Biochem.* **83**, 205–214 (1978).
- 443 41. Xie, Y. F., MacDonald, J. F. & Jackson, M. F. TRPM2, calcium and neurodegenerative
444 diseases. *International Journal of Physiology, Pathophysiology and Pharmacology* **2**,
445 95–103 (2010).
- 446 42. Fonfria, E. *et al.* TRPM2 is elevated in the tMCAO stroke model, transcriptionally
447 regulated, and functionally expressed in C13 microglia. *J. Recept. Signal Transduct.*
448 *Res.* **26**, 179–198 (2006).
- 449 43. Yang, K.-T. *et al.* Activation of the transient receptor potential M2 channel and
450 poly(ADP-ribose) polymerase is involved in oxidative stress-induced cardiomyocyte
451 death. *Cell Death Differ.* **13**, 1815–1826 (2006).

452

453 **Figure legends for main text**

454 **Fig. 1 ADPR analogues activate TRPM2 in whole cell patch clamp experiments.** Outward
455 currents at +15 mV were recorded as detailed in Methods section. Pipette concentration for
456 ADPR and ADPR analogues was 100 $\mu\text{mol/L}$ in most cases; exceptions are indicated. Data
457 for 30 $\mu\text{mol/L}$ 2'-deoxy-ADPR are from the same experiment as in Fig 2a. Shown are
458 maximum currents from individual patched cells, with the total number of cells indicated.
459 Recordings have usually been performed on multiple days. The median current from all cells
460 of one condition is indicated by a horizontal line. Since in some cases the number of data
461 points was too small to test for normality, data were analyzed by a nonparametric one-way
462 ANOVA (Kruskal–Wallis test) followed by comparison against buffer control, applying
463 Dunn's correction for multiple testing. Results significantly different from buffer control
464 ($p < 0.05$) are indicated by an asterisk. The pipette solution for squaryl and triazole compounds
465 contained 0.1% DMSO; thus, 0.1% DMSO was also used for control conditions. (ADPR -
466 adenosine 5'-diphosphoribose; AMP - adenosine 5'-monophosphate; ASqR - adenosine
467 squaryl ribose; ATPR - adenosine 5'-triphosphate ribose; IDPR - inosine-5'-diphosphoribose;
468 Sal-AMS - salicyl-adenosine monosulfamide, 8-pCPT-AMP - 8-(4-
469 Chlorophenylthio)adenosine-5'-O-monophosphate; 8-Ph-ATrR - 8-Phenyl-adenosine-1,4-
470 triazole ribose). Abbreviations for ligands evaluated are consistent with those in reference ¹³.
471 Analogue structures shown are examples, see Supplementary Fig. 1-4 for all structures.

472

473 **Fig. 2 Modifications of the proximal ribose affect the ability of ADPR to activate**
474 **TRPM2. a,** Concentration response relationship for activation of TRPM2 by ADPR, 2'-
475 deoxy-ADPR, 3'-deoxy-ADPR and 2'-phospho-ADPR in HEK293 cells expressing hTRPM2.
476 Pipette solution contained 200 nmol/L free Ca^{2+} . In the NMDG-based bath solution TRPM2

477 showed characteristic reversal potential and outward rectification (Suppl. Fig. 5a). Currents
478 are displayed as mean±SEM (n= 6–12 for ADPR, 5–6 for 2'-phospho-ADPR, 5–12 for 2'-
479 deoxy-ADPR, 5–9 for 3'-deoxy-ADPR). **b**, Concentration response relationship for activation
480 of endogenous TRPM2 in Jurkat cells. In the NaCl-based bath solution the current showed the
481 reversal potential and I-V relationship of a non-selective cation channel (Suppl. Fig. 5b).
482 Currents are displayed as mean ±SEM (n=2–13 for ADPR, 2–21 for 2'-deoxy-ADPR). Result
483 from a single cell with 250 μmol/L 2'-deoxy ADPR in parenthesis (not included in the
484 concentration response curve). The current axis is shown in reversed orientation to facilitate
485 comparison with panel a. **c**, Ca²⁺-dependence of TRPM2 activation by ADPR and 2'-deoxy
486 ADPR. Concentration response curves for ADPR and 2'-deoxy-ADPR with 50 nmol/L free
487 Ca²⁺ in the pipette solution are shown in addition to the curves with 200 nmol/L from panel a.
488 Currents are displayed as mean±SEM (at 50 nM Ca²⁺ n=2–6 for ADPR, 3–7 for 2'-deoxy-
489 ADPR for 200 nM Ca²⁺ see panel **a**). In all panels n refers to the number of cells recorded for
490 the respective condition, recordings have been performed over multiple days.

491

492 **Fig. 3 Impact of 2'-deoxy-ADPR on hTRPM2 in excised inside-out patches.** **a**, Current
493 steps of hTRPM2 activated by 100 μmol/L ADPR at different potentials. **b**, I-V relationship
494 from patches containing TRPM2 wt or TRPM2 T5L activated by either 100 μmol/L ADPR
495 or 2'-deoxy-ADPR in the presence of 1 μmol/L free Ca²⁺ (n=6-17 patches for TRPM2 wt and
496 n=2–3 patches for TRPM2 T5L). **c**, Single channel slope conductance γ obtained by linear
497 regression of the data in panel b. (unpaired, two-tailed T-tests of the mean±SEM obtained
498 from linear regression, p values are indicated) **d**, Representative continuous recordings of
499 excised inside out patches with the bath solution containing either 100 μmol/L ADPR or 2'-
500 deoxy-ADPR. **e-h, Quantitative analysis of continuous recordings from excised inside-out**
501 **patches e**, Histograms of time to inactivation of wild type TRPM2 after activation by ADPR

502 or 2'-deoxy ADPR with exponential fit. **f**, Decay constants for the time to inactivation. (extra
503 sum-of-squares F-Test, $p=0.0012$). **g**, Average open probability after activation by ADPR or
504 2'-deoxy-ADPR. Whiskers indicate min and max, horizontal bar represents the median
505 (Mann-Whitney test, $p < 0.0001$). **h**, Maximum number of simultaneously active channels in
506 an excised patch after application of either ADPR or 2'-deoxy-ADPR. (unpaired two-tailed T-
507 test, < 0.0001). **a-h** If not indicated otherwise, data are shown as mean \pm SEM. Numbers
508 indicated in the bars refer to the number of patches recorded, usually over multiple days.
509 Significant differences are indicated by asterisks.

510

511 **Fig. 4 NMNAT-2 and CD38 synthesize 2'-deoxy-ADPR *in vitro*.** **a**, β -NMN and 2'-deoxy-
512 ATP were incubated with recombinant hNMNAT-2 and reaction products analyzed by HPLC.
513 2'-deoxy-AMP and 2'-deoxy-ADP were impurities contained in commercial 2'-deoxy-ATP. **b**,
514 Saturation plot for ATP and 2'-deoxy-ATP as substrates of NMNAT-2; β -NMN was used at
515 $290\mu\text{mol/L}$ for both ATP and 2'-deoxy-ATP. Initial reaction rate was calculated from the
516 amount of product formed, determined by HPLC (mean \pm SD ($n=3$ independent experiments
517 with the concentration range shown for ATP, for 2'-deoxy-ATP 3 additional experiments were
518 performed for 3 mM, 5 mM, 7 mM and 9 mM, therefore $n=6$ for 3 mM and 9 mM)). Data for
519 ATP were fitted to a Michaelis-Menten model. Data up to 3 mmol/L 2'-deoxy-ATP were
520 fitted to a Hill model. At higher concentrations the reaction rate dropped rapidly, indicating
521 substrate inhibition (dashed line). **c**, Recombinant hCD38 hydrolyzed 2'-deoxy-NAD (from
522 panel a) to yield the TRPM2 agonist 2'-deoxy-ADPR (a+c are representative for three
523 independent experiments). **d**, CD38 activity was determined by incubation of Jurkat cells with
524 $1,N^6$ -etheno-NAD and HPLC analysis of product $1,N^6$ -etheno-ADPR at different time points.
525 To analyze CD38 activity in type III orientation (red symbols), CD38 activity on the cell

526 surface was inhibited by covalently bound araF-NAD (blue symbols turned into gray). To
527 obtain access to type III CD38, the plasma membrane was selectively permeabilized using
528 saponin. After determination of type III CD38 activity, cells were incubated with araF-NAD
529 again (red symbols turned into gray). Data are shown as mean±SEM. The number of
530 experiments is indicated. For conditions tested in a one-way ANOVA for repeated
531 measurements, using Tukey's corrections for multiple testing, the corrected p values are
532 shown.

533

534 **Fig. 5 The increase in 2'-deoxy-ADPR in Jurkat cells exposed to hydrogen peroxide**
535 **depends on CD38.** Wild type and CD38^{-/-} Jurkat cells were either exposed to 100 μmol/L
536 H₂O₂ for 5 min or left unstimulated. **a+d** Deproteinized extracts from cell samples were
537 separated by RP-HPLC on Phenomenex Luna C8 column and fractions co-eluting with
538 authentic ADPR, NAD, 2'-deoxy-ADPR or 2'-deoxy-NAD were collected. **b+c+e+f** Fractions
539 from the pre-fractionation on C8 column were subjected to a second dimension of RP-HPLC
540 on Multohyp BDS-C18 5μ column. To correctly assign peaks, each sample was split and one
541 half was spiked with the respective nucleotide (gray tracings). Representative chromatograms
542 for each condition are shown. Since we could not achieve baseline separation for 2'-deoxy-
543 ADPR, it was not analyzed quantitatively, however, the peak of 2'-deoxy-ADPR clearly
544 increased upon hydrogen peroxide stimulation. In the chromatograms from CD38^{-/-} cells the
545 respective peak was not detected, regardless of stimulation. **g**, Quantitative analysis of the
546 impact of H₂O₂ on intracellular 2'-deoxy-NAD. Independent experiments were initiated on 3
547 separate days over the course of one month, with each experiment consisting of multiple
548 parallel cell preparations. 2–6 data points were obtained per experimental day. Results from
549 single experiments are indicated as filled circles (horizontal lines indicate the mean) with the
550 same shade of gray signifying individual experiments from a single day. Data are normally

551 distributed in each group. Analysis by one-way ANOVA did not reveal significant differences
552 for 2'-deoxy-NAD ($p=0.074$).

553

554 **Fig. 6 Concentration of 2'-deoxy ADPR in Jurkat cells increased after exposure to**
555 **hydrogen peroxide. a**, Deproteinized cell extracts from either unstimulated Jurkat cells or
556 Jurkat cells exposed to 100 $\mu\text{mol/L}$ H_2O_2 were applied to a Phenomenex Luna C8 column and
557 a fraction co-eluting with chemically synthesized 2'-deoxy ADPR (R_t between 24 and 25 min)
558 was collected **a + b**, The fractions were further chromatographed on a Multohyp BDS-C18 5 μ
559 column. To confirm identity of the peak co-eluting with standard 2'-deoxy ADPR (dashed
560 tracing), samples were also spiked with 15.6 nmol 2'-deoxy ADPR (gray tracing). The slight
561 enhancement of the spiked peak is in agreement with the amount of 2'-deoxy-ADPR added as
562 spike (see standard trace for comparison). **d**, Quantitative analysis of the impact of H_2O_2 on
563 intracellular 2'-deoxy ADPR (per 10^7 cells). Results from single experiments are indicated as
564 gray symbols (horizontal lines indicating median value) with symbols of same shape and gray
565 level signifying experiments from the same day. The number of independent preparations and
566 the number of days (12 samples from 3 days for H_2O_2 stimulated cells vs 47 samples from 7
567 days for unstimulated cells) are indicated in the chart. Due to non-normal distribution, data
568 were analyzed by a nonparametric Mann-Whitney test.

569

570 **Online Methods**

571 *Chemical Synthesis and Purification of ADPR Analogues*

572 Chemical synthesis, purification and characterization of 2'-deoxy-ADPR, 3'-deoxy-ADPR and
573 all other non-commercial ADPR analogues, apart from hydroxyl-ethoxy-ethyl-ASq, was as

574 described previously^{13,44,35}. Analogue identity was confirmed by ¹H-NMR and HRMS. Purity
575 was checked by HPLC (>95%) and re-checked after storage.

576 *Synthesis of hydroxyl-ethoxy-ethyl-ASq*

577 *3-(2-(2-hydroxyethoxy)ethylamino)-4-ethoxycyclobut-3-ene-1,2-dione*

578 To a solution of 2-(2-aminoethoxy)ethanol (95 μ L, 0.951 mmol) and DIPEA (81 μ L, 0.467
579 mmol) in EtOH (8 mL) was added diethylsquarate (128 μ L, 0.865 mmol). After 1h, the
580 solvent was removed under reduced pressure and the residue was purified on an Isco
581 chromatographic system (DCM-acetone, 8:2 v/v) to yield the desired product as a colorless oil
582 (165 mg, 91%). ¹H (400 MHz, *d*₄-MeOH) δ 4.79 (q, 2H, *J* = 7.1 Hz, OCH₂-Me), 3.85-3.61
583 (m, 8H, 4 x CH₂) and 1.51 (t, 3H, *J* = 7.1 Hz, CH₃). ¹³C (100 MHz, *d*₄-MeOH) δ 189.9 (C-2),
584 184.9 (C-1), 177.9 (C-3), 175.1 (C-4), 73.5, 70.9 (both CH₂), 70.7 (Et: CH₂), 62.2, 45.5 (both
585 CH₂) and 16.2 (Et: CH₃). HRMS (ES⁺) calcd for C₁₀H₁₆NO₅ 230.1023 (MH)⁺ found
586 230.1031.

587 *3-(2',3'-O-Isopropylidene-5'-amino-5'-deoxyadenosine)-4-(2-(2-hydroxyethoxy)ethyl-*
588 *amino)cyclobut-3-ene-1,2-dione*

589 To a solution of 3-(2-(2-hydroxyethoxy)ethylamino)-4-ethoxycyclobut-3-ene-1,2-dione (60
590 mg, 0.287 mmol) and DIPEA (27 μ L, 0.154 mmol) in EtOH-DMF (1:1 v/v, 1 mL) was added
591 2',3'-isopropylidene-5'-amino-5'-deoxyadenosine (96 mg, 0.315 mmol). After 26h, the solvent
592 was removed under reduced pressure and the residue was purified on an Isco chromatographic
593 system (DCM-MeOH, 8:2 v/v) to yield the desired product as a white foam (104 mg, 74%).
594 ¹H (400 MHz, *d*₆-DMSO) δ 8.30 (s, 2H, H-8 and H-2), 6.24 (d, 1H, *J*_{1',2'} = 2.6 Hz, H-1'), 5.55
595 (dd, 1H, *J*_{2',3'} = 6.4 and *J*_{2',1'} = 2.6 Hz, H-2'), 5.16 (dd, 1H, *J*_{3',2'} = 6.4 and *J*_{3',4'} = 3.7 Hz, H-3'),
596 4.44-4.41 (m, 1H, H-4'), 4.07-4.04 (m, 1H, H-5'a), 3.94 (dd, 1H, *J*_{5'b,5'a} = 14.1 and *J*_{5'b,4'} = 6.6
597 Hz, H-5'b), 3.78 (brs, 2H, CH₂-O), 3.72-3.70 (br, 2H, CH₂-NH), 3.64 (brs, 2H, CH₂-O), 3.61-

598 3.59 (m, 2H, CH₂-OH), 1.65 (s, 3H, CH₃) and 1.44 (s, 3H, CH₃). ¹³C (100 MHz, *d*₆-DMSO) δ
599 184.2 (C-2), 183.3 (C-1), 169.6 (both C=C), 157.6 (C-6), 154.3 (C-2), 150.3 (C-4), 142.0 (C-
600 8), 120.7 (C), 115.9 (C-5), 91.5 (C-1'), 87.0 (C-4'), 85.1 (C-2'), 82.9 (C-3'), 73.6, 71.4, 62.1,
601 46.7 (all CH₂), 45.1 (C-5'), 27.6 and 25.6 (both CH₃). HRMS (ES⁺) calcd for C₂₁H₂₈N₇O₇
602 490.2045 (MH)⁺ found 490.2027.

603 *3-(5'-amino-5'-deoxyadenosine)-4-(2-(2-hydroxyethoxy)ethylamino)cyclobut-3-ene-1,2-dione*
604 **(23)**

605 3-(2',3'-*O*-Isopropylidene-5'-amino-5'-deoxyadenosine)-4-(2-(2-hydroxyethoxy)ethylamino)-
606 cyclobut-3-ene-1,2-dione (80 mg, 0.163 mmol) was stirred in a 75% aq. TFA solution (5 mL)
607 at rt for 1h. The solvents were evaporated under reduced pressure and the residue co-
608 evaporated with MeOH to remove any residual TFA. The remaining residue was purified on
609 an Isco purification system (DCM-MeOH, 8:2 v/v) to yield the desired compound as a white
610 solid (60 mg, 82%). ¹H (400 MHz, *d*₆-DMSO) δ 8.39 (s, 1H), 8.22 (s, 1H), 7.57 (br s, 2H),
611 7.37 (br s, 2H, NH₂), 5.97 (d, 1H, *J*_{1',2'} = 5.8 Hz, H-1'), 5.62 (d, *J* = 6.1 Hz, 2'-OH), 5.44 (d, *J*
612 = 4.8 Hz, 3'-OH), 4.75 (ddd, 1H, *J*_{2',3'} = 6.4, *J*_{2',OH} = 6.1, *J*_{2',1'} = 5.8 Hz, H-2'), 4.67 (t, *J* = 5.3,
613 OH), 4.21 (ddd, 1H, *J*_{3',2'} = 6.4, *J*_{3',OH} = 4.8, *J*_{3',4'} = 4.0 Hz, H-3'), 4.08-4.05 (m, 2H, H-4', H-
614 5'a), 3.85-3.80 (m, 1H, H-5'b), 3.69 (brs, 2H, CH₂-O), 3.56-3.49 (m, 6H, 3 × CH₂). ¹³C (125
615 MHz, *d*₆-DMSO) δ 182.6 (C-2), 182.4 (C-1), 167.8 (both C=C), 156.1 (C-6), 152.7 (C-2),
616 149.4 (C-4), 139.8 (C-8), 119.2 (C-5), 87.4 (C-1'), 83.6 (C-4'), 72.7 (C-2'), 72.1 (CH₂), 70.8
617 (C-3'), 70.0, 60.1 (both CH₂), 45.5 (C-5'), 43.2 (CH₂). HRMS (ES⁺) calcd for C₁₈H₂₄N₇O₇
618 450.1737 (MH)⁺ found 450.1730.

619

620 *Commercial ADPR Analogues*

621 2'-phospho-ADPR (**15**), 1,N⁶-etheno-ADPR (**12**), and 8-(4-Chlorophenylthio)adenosine-5'-
622 mono-phosphate (8-pCPT-AMP, **32**) were purchased from Biolog.

623 *Cell Culture*

624 Jurkat subclone JMP with high expression of CD3 was originally generated at University of
625 Erlangen, Medical Faculty, Erlangen, Germany. They were recently authenticated as Jurkat by
626 short tandem repeats (STR) profiling and tested negative for contamination with rodent cells
627 (DSMZ service for the authentication of human cell lines). Jurkat cells were cultured as
628 described before⁴⁵. Briefly, cells were kept in RPMI-1640 with GlutaMax-I and 25 mM 4-(2-
629 hydroxyethyl)-1-piperazineethanesulfonic acid (HEPES) supplemented with 7.5% newborn
630 calf serum (FCS) and penicillin (100 units/mL)/streptomycin (100 µg/mL). Cell density was
631 kept between 0.3x10⁶ and 1.0x10⁶/ml. For determination of endogenous concentrations of 2'-
632 deoxy-ADPR which required large amounts of cells, Jurkat cells were cultivated in spinner
633 bottles at a cell density of up to 1.0x10⁶ cells/mL.

634 HEK293 Tet-On cells were obtained from Clontech/Takara. Wild type HEK293 cells were
635 kindly provided by Prof. Dr. Manfred Jücker (Department of Biochemistry and Signal
636 Transduction, University Medical Centre Hamburg-Eppendorf, Germany). HEK293 cells
637 were kept in DMEM medium with 4.5 g/L D-glucose and without pyruvate supplemented
638 with 10% fetal calf serum, 100 units/mL penicillin, and 100 µg/mL streptomycin. For
639 maintenance of HEK293 cell lines TRPM2#24 and EGFP#8 400 µg/mL G418-sulfate was
640 added to the medium. For the maintenance of HEK293 Tet-On cell line expressing the
641 TRPM2 T5L mutant medium was supplemented with 100 µg/mL G418 sulfate and 25 µg/mL
642 hygromycin B. All cells were kept at 37°C and 5% CO₂. HEK293 cells are a well-established
643 system for the electrophysiological characterization of recombinant ion channels. They
644 express very little endogenous ion channels that might confound measurements and patch
645 clamp experiments are straightforward since cells tend to seal very well. To avoid the risk of

646 using cross-contaminated cells the parental wild type HEK293 cells and the HEK293 Tet-On
647 cell line expressing the T5L mutant of hTRPM2 were authenticated by STR profiling and
648 tested negative for contamination with rodent cells (DSMZ service for the authentication of
649 human cell lines). All cells were tested for mycoplasma contamination on a regular basis
650 using an enzymatic assay (MycoAlert™ Mycoplasma Detection Kit, Lonza).

651 *Generation of HEK293 Cell Lines*

652 Generation of HEK293 cells with stable expression of hTRPM2 and EGFP (TRPM2 #24) has
653 been described before¹³. The complete open reading frame of wild type hTRPM2 was
654 amplified from the expression vector pIRES2-EGFP-TRPM2 described previously⁴⁵ using the
655 primers 5'-GGAATTCCGCCACCATGGAGCCCTCAGCCCTG-3' and 5'-
656 TACTGTCGACTCAGTAGTGAGCCCC-3'. *EcoRI* and *SalI* sites in the primers allowed for
657 integration of the amplicon into the respective sites of the multiple cloning site of pTRE-tight
658 (Clontech/Takara). The mutation T5L described by Tóth and coworkers²⁰ was introduced by
659 QuikChange mutagenesis (Stratagene/Agilent) using the primers 5'-
660 GGCCAGATCCCGCTGGACGAGATCGACGGTGTGAACTTC-3' and 5'-
661 GAAGTTCACACCGTCGACTCGTCCAGCCGGGATCTGGCC-3'. The complete open
662 reading frame was confirmed by DNA sequencing (MWG Eurofins). HEK 293 Tet-On cells
663 (Clontech/Takara) were co-transfected with pTRE-tight-TRPM2 T5L and pTK-Hyg
664 (Clontech/Takara). Transfectants were selected by adding 25 µg/mL hygromycin B to the
665 culture medium. Clonal cell lines for further analysis were generated from surviving cells by
666 limiting dilution and chosen according to their response to hydrogen peroxide as described
667 before¹³. While two clones showed a calcium signal in response to hydrogen peroxide, neither
668 was inducible by doxycycline. Excised inside/out patches from both clones showed ADPR
669 inducible currents with a higher single channel conductance than wild type TRPM2 as was
670 expected for the T5L mutant.

671 *Whole Cell Patch Clamp Analysis of TRPM2 Activation*

672 Whole cell patch clamp experiments were performed as described previously^{13,46}. Briefly,
673 HEK293 cells with stable expression of human TRPM2 were seeded to 35 mm dishes. The
674 day after medium was removed and replaced by bath solution (140 mM N-methyl-D-
675 glucamine (NMDG), 5 mM KCl, 3.3 mM MgCl₂, 1 mM CaCl₂, 5 mM D-glucose, 10 mM
676 HEPES, pH 7.4 adjusted with HCl). Patch pipettes with a resistance of 1.5 to 3.5 MΩ were
677 pulled from thin-walled 1.5 mm diameter borosilicate (1.10 mm x 1.50 mm x 80 mm) glass
678 capillaries and filled with pipette solution (120 mM KCl, 8 mM NaCl, 1 mM MgCl₂, 10 mM
679 HEPES, 10 mM ethylene glycol-bis(β-aminoethyl ether)-N,N,N',N'-tetraacetic acid (EGTA),
680 the concentration of free Ca²⁺ ions in the pipette solution was buffered to 50 nM or 200 nM
681 by addition of either 2.3 mM or 5.6 mM CaCl₂ as calculated by Maxchelator:
682 <http://maxchelator.stanford.edu/CaEGTA-NIST.htm>). Currents were compensated for fast and
683 slow capacity transients and recorded using an EPC10 amplifier and PatchMaster software
684 (HEKA Elektronik). Series resistance was compensated by 70%. Voltage ramps from -85 mV
685 to +20 mV in 140 ms were applied every 5 s over a period of 450 s starting from a holding
686 potential of -50 mV. For analysis the maximum outward current at +15 mV during the course
687 of experiment was extracted from all experiments. In the NMDG-based bath solution the I-V
688 curve of TRPM2 showed characteristic reversal potential and outward rectification
689 (Supplementary Results, Supplementary Fig. 5a), facilitating differentiation between
690 activation of the non-selective cation channel and leaky cells/patches. If the patch ruptured
691 before peak current was obtained or if significant changes in series resistance occurred during
692 the measurement, recordings were excluded from analysis.

693 Jurkat cells were seeded to 35 mm dishes coated with poly-L-Lysine (MW 70–150kDa,
694 Sigma Aldrich). After cells had adhered to the dish, medium was removed and replaced by
695 bath solution (140 mM NaCl, 2 mM MgCl₂, 2 mM CaCl₂, 5 mM KCl, 10 mM HEPES, and 5

696 mM glucose adjusted to pH 7.4 with NaOH). Pipettes were prepared as described above and
697 filled with pipette solution (140 mM KCl, 2 mM MgCl₂, 2.5 mM EGTA, and 10 mM HEPES
698 adjusted to pH 7.4 with KOH, the concentration of free Ca²⁺ ions in the solution was buffered
699 to 50 nM by addition of 0.59 mM CaCl₂ as calculated by MaxChelator). Currents were
700 recorded as described above. Voltage ramps from -85 mV to +65 mV in 200 ms were applied
701 every 10 s over a period of 300 s starting from a holding potential of -60 mV.

702 *Electrophysiological Recordings from Excised Inside/Out-Patches*

703 Cells with stable expression of either wild type hTRPM2 or hTRPM2 T5L were seeded to
704 35 mm dishes 24–48 h before use. Before the experiments medium was exchanged for a
705 buffer based on sodium gluconate (140 mmol/L Na gluconate, 2 mmol/L MgCl₂, 7.6 mmol/L
706 CaCl₂, 10 mmol/L EGTA, 10 mM HEPES pH7.2, free Ca²⁺ concentration 1 μmol/L). Patch
707 pipettes with resistances of 10–15 MΩ were pulled from thick-walled borosilicate glass
708 capillaries (0.86 mm x 1.50 mm x 80 mm) using a Sutter P-97 and filled with the same
709 solution (symmetrical solutions). 100 nmol/L Tetrodotoxin (TTX) was added to the pipette
710 solution to block endogenous voltage-gated sodium channels⁴⁷. For activation of the channel
711 either ADPR or 2'-deoxy-ADPR was added to the bath solution. After excision of a patch
712 with one or a few channels the fast capacity transients were compensated. For the
713 determination of the average open probability the patch membrane was held at a potential of -
714 60 mV and the current was continuously recorded for a maximum of 30 min. For the
715 determination of the slope conductance the potential across the patch membrane was
716 increased by 20 mV steps every 20 s starting from -60 mV with a delay of 100 ms between
717 steps. Data were sampled at 10 kHz and recorded to disk using the EPC10 amplifier and
718 PatchMaster software (v2.32, HEKA Elektronik). For analysis of the single channel data
719 recordings were filtered to remove 50 Hz mains hum by an electrical interference filter and
720 low-pass-filtered (1 kHz) to remove high-frequency noise. To determine single channel

721 conductance Gaussian distributions were fitted to current histograms of the recordings and
722 voltage steps were calculated as difference between the centers of the distributions. To
723 determine average open probabilities continuous recordings were filtered and base-line
724 corrected and exported to a script for trapezoid integration of the area under the curve written
725 in Python (www.python.org, v2.7) and using the numpy/scipy libraries (www.scipy.org ,
726 numpy v1.8.1 and scipy v0.12.0) for numerical computations. At points of permanent
727 inactivation of channels the recording was split into sections and the sections were separately
728 integrated. The resulting integrals were divided by number of channels, duration and average
729 height of voltage steps at -60 mV. The number of simultaneously open channels in a patch
730 (Fig 3h) was determined either from the steps in the recording or for recordings where
731 identification of individual states was not possible the number of channels was calculated by
732 dividing peak current by single channel current for -60 mV. For display purposes (Fig 3a+d)
733 data was filtered with a 100 Hz low pass filter and down-sampled by a factor of 10.

734 *Production of Recombinant Human CD38*

735 A fragment of the open reading frame of human CD38 encoding amino acids P44 to I300 was
736 amplified using the primers 5'-
737 ATGGTACGTCTCAGGCCCGAGGTGGCGCCAGCAGTG-3' and 5'-
738 ATGGTACGTCTCAGCGCTGATCTCAGATGTGCAAGATGAATC-3'. The amplicon was
739 digested with *Esp3I* and inserted into the *BsaI* site of the multiple cloning site of the
740 eukaryotic expression vector pEXPR-iba42 (Iba). The resulting reading frame encodes an *N*-
741 terminal BM40 signal sequence followed by a 6xHis-Tag, the extracellular part of CD38 and
742 a *C*-terminal Strep-Tag. This open reading frame was confirmed by DNA sequencing (MWG
743 Eurofins). HEK293 cells were transfected with the expression vector and transfectants were
744 selected by addition of 400 μ g/mL G418-sulfate to the culture medium. The bulk of surviving
745 cells was continuously kept as described above and the supernatant medium was collected

746 each time cells were sub-cultured. Soluble recombinant CD38 secreted by the cells was
747 purified from the pooled supernatant by affinity chromatography using Ni-NTA agarose
748 (Qiagen). Imidazole was removed from elution fractions by dialysis and the protein solution
749 concentrated by ultrafiltration.

750 *Enzymatic Synthesis of 2'-deoxy-NAD*

751 5 mmol/L β -NMN and 5 mmol/L 2'-deoxy ATP were incubated at 37°C with 1 μ g/mL
752 recombinant human NMNAT-2 (R&D Systems) overnight. The enzyme was removed
753 afterwards by passing the sample through a centrifugal filter device with 10 kDa cutoff. The
754 sample volume was reduced using a SpeedVac evaporator. Separation of the product 2'-
755 deoxy-NAD from byproducts and remaining substrates was achieved by HPLC using a
756 250 mm \times 10 mm Luna C8 5 μ m column (Phenomenex) equipped with a 10 mm \times 10 mm guard
757 cartridge containing a C8 ODS filter element (Phenomenex) at a flow rate of 2.5 mL/min with
758 the buffer (50 mmol/L ammonium acetate, 0.05% acetic acid, pH 5.4) containing increasing
759 amounts of methanol as outlined below. The fraction co-eluting with chemically synthesized
760 2'-deoxy-NAD was collected, dried using a SpeedVac evaporator, reconstituted in water and
761 checked for purity by HPLC as outlined below. Concentration of the solution was adjusted
762 against chemically synthesized 2'-deoxy-NAD.

763 *HPLC-based Enzyme Assays for NMNAT-2 and CD38*

764 Recombinant human NMNAT-2 (R&D Systems) at a concentration of 5 ng/ μ L was incubated
765 for 15 min at 37°C with 290 μ mol/L β -NMN and 2.5 mmol/L 2'-deoxy-ATP in assay buffer
766 (50 mmol/L Tris, 10 mmol/L MgCl₂, pH 7.6). Afterwards the enzyme was removed by
767 passing the samples through centrifugal filter devices with 10 kDa cutoff. Reaction products
768 were analyzed via reversed-phase ion pair (RP)-HPLC on a Multohyp BDS-C18 5 μ column
769 (250 mm x 4.6 mm, particle size 5 μ m, CS Chromatographie Service) equipped with a
770 security guard cartridge (4 mm x 3.0 mm) containing a C18 ODS filter element (Phenomenex)

771 at a flow rate of 0.8 mL/min with the buffer (20 mmol/L KH_2PO_4 , 5 mmol/L
772 tetrabutylammonium dihydrogen phosphate, pH 6) containing increasing amounts of
773 methanol. The methanol gradient was: 0 min (15%), 3.5 min (15%), 11 min (31.25%), 15 min
774 (31.25%), 25 min (50%), 27 min (50%), 29 min (15%) and 38 min (15%). The DAD (Diode-
775 Array detector, Agilent Technologies) was set to 260 nm for detection of nucleotides. Peak
776 integration was performed using ChemStation Software (Rev. C.01.05, Agilent
777 Technologies).

778 Peaks co-eluting with chemically synthesized 2'-deoxy-NAD were collected and methanol
779 was removed on a SpeedVac evaporator. Afterwards pH was adjusted to 7.2 and the MgCl_2
780 concentration to 1 mmol/L. Part of the sample was incubated for 1 h at 37°C with
781 0.33 Units/mL nucleotide pyrophosphatase from *Crotalus adamanteus*. The remainder of the
782 sample was incubated with a recombinant soluble form of human CD38 for 15 min at 37°C.
783 The putative 2'-deoxy-ADPR peak from the CD38 reaction was collected for pyrophosphatase
784 digest. In all cases the products were analyzed via reversed-phase ion pair HPLC as described
785 above.

786 *Substrate saturation plots*

787 To create substrate saturation plots of human NMNAT-2 for the substrates ATP and 2'-deoxy-
788 ATP, 30 ng recombinant NMNAT-2 (R&D Systems) was incubated in 100 μl reaction buffer
789 (25 mmol/L KH_2PO_4 , 5 mmol/L DTT, 20 mmol/L MgCl_2 , 0.5 mg/ml bovine serum albumin
790 (BSA), adjusted to pH 7.5 with KOH) with different concentrations of the substrates (ATP, 2'-
791 deoxy-ATP). For soluble recombinant human CD38, 0.5 ng or 1.0 ng of the enzyme
792 (produced as described above) was incubated in 100 μl reaction buffer (110 mmol/L KCl,
793 5 mmol/L KH_2PO_4 , 10 mmol/L NaCl, 2 mmol/L MgCl_2 , 20 mmol/L HEPES, pH 7.2 mit
794 KOH) with different concentrations of either NAD or 2'-deoxy-NAD as substrate for 20 min

795 at 37°C. Reactions were stopped by cooling the samples rapidly to nearly 0°C and removing
796 the enzyme by centrifugation through a 10 kDa filter device (VivaSpin, Sartorius) at 4°C. The
797 amount of product formed was determined by HPLC analysis as described above using
798 external standards for quantification. In case of CD38 substrate solutions contained minor
799 contaminations of either ADPR / 2'-deoxy-ADPR that were subtracted before kinetic
800 parameters for the enzyme/substrate pairs were calculated using GraphPad Prism (v6.03,
801 GraphPad Software).

802 *Immunoprecipitation and western blot analysis of poly-ADP-ribosylated proteins*

803 HEK-293 cells were seeded to 150 mm dishes. Four days later at 80-90% confluence medium
804 was replaced by pre-warmed buffer (15 mmol/L HEPES, 140 mmol/L NaCl, 5 mmol/L KCl,
805 1 mmol/L MgCl₂, 10 mmol/L Glucose, 1.8 mmol/L CaCl₂, pH 7.4) and hydrogen peroxide
806 was added to a final concentration of 1 mmol/L. After 5 min buffer was replaced by pre-
807 warmed phosphate buffered saline (137.93 mmol/L NaCl, 2.67 mmol/L KCl, 8.06 mmol/L
808 Na₂HPO₄, 1.47 mmol/L KH₂PO₄, 0.493 mmol/L MgCl₂, 0.901 mmol/L CaCl₂, pH 7.38) and
809 cells were washed twice. Lysis of cells and isolation of poly ADP-ribosylated proteins was
810 based on Gagné et al⁴⁸. Dishes were put on ice and 2 mL lysis buffer (40 mmol/L HEPES,
811 120 mmol/L NaCl, 1 mmol/L EDTA, 0.3% CHAPS (w/v), pH 7.5) with protease inhibitor
812 (Roche complete, EDTA-free) and PARG inhibitor ADP-HPD (Enzo Life Sciences) was
813 added to the cells which then were detached from the dishes and kept on ice for 15 min and on
814 overhead rotation at 4°C for an additional 20 min. Non-lysed cells were removed by
815 centrifugation. Paramagnetic beads were washed twice with sodium acetate buffer (0.1 mol/L
816 Na acetate, pH 5.0) and incubated 30 min at 4°C with either anti-pADPR antibody (10H,
817 Abcam # ab14459) or mouse normal IgG (Thermo Fisher Scientific) in PBS-T (PBS, 0.02%
818 Tween20 (v/v)) on overhead rotation. Non-specific binding was prevented by incubation with
819 blocking buffer for 1 h at room temperature. Directly before addition to the lysed cells beads

820 were washed with lysis buffer with protease inhibitor. Beads were incubated with the cell
821 lysate for 2 h at 4°C on overhead rotation and washed five times with lysis buffer. For
822 Western blot analysis poly-ADP-ribosylated proteins were eluted from the beads by
823 incubation in sample buffer (0.22 mol/L Tris, 22.6% (v/v) glycerol, 4% (w/v) SDS, 5.3%
824 (v/v) 2-mercapto ethanol, pH6.8) at 65°C for 5 min. Afterwards proteins were separated by
825 10% SDS-PAGE and transferred to a PVDF membrane (Merck, Darmstadt) by tank blotting.
826 The membrane was blocked in TBS-MT (50 mmol/L Tris, 150 mmol/L NaCl, pH 7.6, 0.1%
827 Tween20 (v/v), 5% dry milk protein(w/v)) and incubated overnight at 4°C with the primary
828 anti-PAR antibody (pADPR antibody from rabbit, R&D Systems/Bio-Techne #4336-APC-
829 050) diluted 1:1000 in TBS-MT. The secondary goat anti-rabbit antibody conjugated to
830 horseradish peroxidase (HRP) (Dianova #111-035-045) was applied in 1:10 000 dilution in
831 TBS-MT. HRP was detected by chemoluminescence using an Image Quant
832 LAS4000/LAS3000 (GE Healthcare Life Sciences) after incubation of the membrane in
833 SuperSignal Working Solution (Thermo Fisher Scientific) for 5 min.

834 *PARG hydrolysis of poly-ADP-ribosylated proteins and HPLC analysis of products*

835 Beads with poly-ADP ribosylated proteins were washed in phosphate buffer (20 mmol/L
836 KH₂PO₄, pH 7.2), resuspended in 100 µl phosphate buffer + 10 mmol/L MgCl₂ and after
837 addition of 100 ng recombinant human PARG (Adipogen International) incubated for 2.5 h at
838 37°C. After removal of beads and PARG by passing the samples through centrifugal filter
839 devices with 10kD cutoff, 1 µL citric acid, 1 µL chloroacetaldehyde and 33 µL water were
840 added to 85 µL of the sample and incubated for 40 min at 80°C resulting in conversion of the
841 adenine nucleotides to the respective fluorescent 1, N⁶-etheno compounds. Analysis of the
842 converted nucleotides was based on the method described by Bobalova et al.⁴⁹ HPLC analysis
843 was performed on either a 1200 Series system or a 1260 Infinity system (both Agilent
844 Technologies) using a 250 mm×4.6 mm Multohyp BDS-C18 5µ column (CS

845 Chromatographie Service) equipped with a 4.0mm×3.0mm guard cartridge containing a C18
846 ODS filter element (Phenomenex) at a flow rate of 0.8 mL/min with the buffer (100 mmol/L
847 KH₂PO₄, pH 6) containing increasing amounts of methanol. The gradient was: 0 min (0%
848 methanol), 22.5 min (35% methanol), 25 min (35% methanol), 29 min (0% methanol) and
849 38 min (0% methanol). Fluorescence of 1, N⁶-ethenoadenosine was detected at an emission
850 wavelength of 410 nm after excitation at 230 nm. Peaks were integrated using ChemStation
851 Software (Rev. C.01.05) from Agilent Technologies. Quantification was performed using
852 external standards.

853 *Assay for type III CD38 activity using permeabilized cells*

854 10⁶ wildtype Jurkat cells or CD38^{-/-} Jurkat cells were washed, resuspended in 200 µl reaction
855 buffer (140 mmol/L NaCl, 5 mmol/L KCl, 1 mmol/L NaH₂PO₄, 1 mmol/L MgSO₄, 1 mmol/L
856 CaCl₂, 5.5 mmol/L Glucose, 20 mmol/L HEPES, pH7.4 with NaOH) and incubated with 1,
857 N⁶-etheno-NAD at a final concentration of 50 µmol/L. Reaction was stopped after 0, 5, 10, 15
858 and 30 min by spinning down the cells and passing the supernatant through a centrifugal filter
859 device with 10kD cutoff. Samples were analysed by HPLC using fluorescence detection as
860 described below, to determine the amount of 1, N⁶-etheno-ADPR formed. Reaction rates were
861 calculated from the increase in product by linear regression. To block the activity of CD38 on
862 the cell surface, cells were incubated in 1 µmol/L araF-NAD in reaction buffer for either
863 40 min or 90 min at RT. Excess araF-NAD was removed by washing the cells in reaction
864 buffer prior to the determination of the CD38 activity. To selectively permeabilize the plasma
865 membrane 10⁶ cells were washed once in intracellular buffer (120 mmol/L KCl, 10 mmol/L
866 NaCl, 1.2 mmol/L MgCl₂, 0.533 mmol/L CaCl₂, 10 mmol/L HEPES, 1 mmol/L EGTA, pH7.2
867 with KOH) and resuspended in intracellular buffer with 90 µg/mL saponin. After incubation
868 at 37°C for 5 min cells were washed in nominally Ca²⁺ free intracellular buffer (120 mmol/L
869 KCl, 10 mmol/L NaCl, 1.2 mmol/L MgCl₂, 10 mmol/L HEPES, pH7.2 with KOH) twice

870 before CD38 activity was determined using 1, *N*⁶-etheno-NAD as described above. To test
871 whether residual activity was due to CD38, permeabilized cells were also incubated with
872 1 μmol/L araF-NAD for 40 min at RT. Excess araF-NAD was removed by washing the cells
873 prior to the determination of the CD38 activity as described above.

874

875 *Quantification of endogenous 2'-deoxy-ADPR by HPLC*

876 1x10⁸ Jurkat cells at a cell density of 1x10⁶ cells/mL were harvested from suspension, washed
877 twice in Ca²⁺ measurement buffer (140 mmol/L, NaCl, 5 mmol/L KCl, 1 mmol/L MgSO₄,
878 1 mmol/L CaCl₂, 1 mmol/L NaH₂PO₄, 5.5 mmol/L D-glucose and 20 mmol/L HEPES, pH
879 7.4) and resuspended in 5 mL of the same buffer. After 25 min at 25°C hydrogen peroxide
880 was added to a final concentration of 100 μmol/L. An additional 2 or 5 minutes later cells
881 were collected by centrifugation and nucleotides extracted from the cells by addition of
882 trichloroacetic acid, freeze/thawing and sonication. Denatured proteins and nucleic acids were
883 removed by centrifugation and 25 pmol 1, *N*⁶-ethenoadenosine was added to the supernatant
884 as internal standard. Trichloroacetic acid was removed by four cycles of extraction with
885 diethyl ether. To remove residual diethyl ether samples were dried using a SpeedVac
886 evaporator and reconstituted in water. After samples were filtered through 0.2 μm syringe
887 filter devices, samples were again dried and reconstituted in 15% methanol/water. HPLC
888 analysis was performed on either a 1200 Series system or a 1260 Infinity system (both Agilent
889 Technologies). The first step of chromatographic separation was run on a 250 mm×10 mm
890 Luna C8 5 μm column (Phenomenex) equipped with a 10 mm×10 mm guard cartridge
891 containing a C8 ODS filter element (Phenomenex) at a flow rate of 2.5 mL/min with the
892 buffer (20 mmol/L KH₂PO₄, 5 mmol/L tetrabutylammonium dihydrogen phosphate, pH 6)
893 containing increasing amounts of methanol. The gradient was: 0 min (15% methanol),
894 3.5 min (15% methanol), 11 min (31.25% methanol), 15 min (31.25% methanol), 25 min

895 (50% methanol), 27 min (50% methanol) , and 29 min (15% methanol). Adenine nucleotides
896 were detected using the DAD (photo diode array detector) at 260 nm. Fluorescence of 1, *N*⁶-
897 ethenoadenosine was detected at an emission wavelength of 410 nm after excitation at
898 275 nm. Two fractions of roughly 2.5 mL were manually collected around the retention times
899 of 1, *N*⁶-ethenoadenosine (*R*_t 13.5 min) and 2'-deoxy-ADPR (*R*_t 24.5 min). Fractions were
900 dried on a SpeedVac evaporator and reconstituted in 15% methanol/water. After
901 reconstitution samples were split into twin samples. For the 2'-deoxy-ADPR fractions one of
902 the samples was spiked with 15.625 pmol 2'-deoxy-ADPR. The second step of
903 chromatographic analysis was run on a 250 mm×4.6 mm Multohyp BDS-C18 5μ column (CS
904 Chromatographie Service) equipped with a 4.0 mm×3.0 mm guard cartridge containing a C18
905 ODS filter element (Phenomenex) at a flow rate of 0.8 mL/min using the same buffer system
906 and detection as above. The gradient was: 0 min (15% methanol), 3.5 min (15% methanol),
907 11 min (31.25% methanol), 15 min (31.25% methanol), 25 min (50% methanol), 27 min
908 (50% methanol) , and 29 min (15% methanol). Peaks were integrated using ChemStation
909 Software (Rev. C.01.05) from Agilent Technologies. Samples with peaks insufficiently
910 resolved for proper integration were excluded. Quantification was performed using external
911 standards. Recovery was determined from the internal standard 1,*N*⁶-ethenoadenosine. Results
912 for 2'-deoxy-ADPR were corrected for recovery.

913

914 *HPLC of endogenous 2'-deoxy-ADPR and 2'-deoxy-NAD for HRMS and quantification of*
915 *endogenous 2'-deoxy-NAD, NAD and ADPR*

916 1x10⁸ wild type Jurkat cells or CD38^{-/-} Jurkat cells per sample were prepared as described
917 above and either left unstimulated or stimulated for 5 min with 100 μmol/L hydrogen
918 peroxide. After deproteination and extraction of the trichloroacetic acid by diethyl ether,
919 samples were dried on a SpeedVac evaporator to remove residual diethyl ether and

920 reconstituted in water. After samples were filtered through 0.2 μm syringe filter devices,
921 samples were again dried on a SpeedVac evaporator and reconstituted in 3% methanol/water.
922 HPLC analysis was performed on either a 1200 Series system or a 1260 Infinity system (both
923 Agilent Technologies). The first step of chromatographic separation was run on a
924 250 mm \times 10 mm Luna C8 5 μm column (Phenomenex) equipped with a 10 mm \times 10 mm guard
925 cartridge containing a C8 ODS filter element (Phenomenex) at a column temperature of 20 $^{\circ}\text{C}$
926 and a flow rate of 2.5 mL/min with the buffer (50 mmol/L ammonium acetate, 0.05% acetic
927 acid, pH 5.4) containing increasing amounts of methanol. The gradient was: 0 min
928 (3% methanol), 5 min (3% methanol), 35 min (50% methanol), 38 min (50% methanol), 45
929 min (3% methanol), and 50 min (3% methanol). Adenine nucleotides were detected as
930 described above. Five fractions of roughly 2.5 mL were manually collected around the
931 retention times of ADPR (R_t 8.2 min), NAD (R_t 12.9 min), 2'-deoxy-ADPR (R_t 13.9 min), 2'-
932 deoxy-NAD (R_t 16.5 min), and 1, N^6 -ethenoadenosine (R_t 24.5 min). All fractions were dried
933 on a SpeedVac evaporator. The fractions containing ADPR, NAD and 1, N^6 -ethenoadenosine
934 were reconstituted in buffer (20 mmol/L KH_2PO_4 , 5 mmol/L tetrabutylammonium dihydrogen
935 phosphate, pH 6 containing 15% methanol) whereas the fractions containing 2'-deoxy-ADPR
936 and 2'-deoxy-NAD were reconstituted in 3% methanol/water. After reconstitution all samples
937 except the ones for 1, N^6 -ethenoadenosine were split into twin samples. One half of the twin
938 sample was spiked with an appropriate amount of the respective nucleotide (ADPR with 100
939 or 250 pmol, NAD with 5 nmol, 2'-deoxy-ADPR with 62.5 pmol and 2'-deoxy-NAD with
940 15.63 pmol). The samples with ADPR, NAD, and 1, N^6 -ethenoadenosine were run on a
941 Multohyp BDS-C18 5 μ column using the same (ion pair) conditions as described above. For
942 the samples with 2'-deoxy-ADPR and 2'-deoxy-NAD which were to be submitted to HRMS
943 the second step of chromatographic analysis was run on a 250 mm \times 4.6 mm Multohyp BDS-
944 C18 5 μ column (CS Chromatographie Service) equipped with a 4.0 mm \times 3.0 mm guard

945 cartridge containing a C18 ODS filter element (Phenomenex) at a column temperature of
946 25°C and a flow rate of 0.8 mL/min with the buffer (50 mmol/L ammonium acetate, 0.05%
947 acetic acid, pH 5.4) containing increasing amounts of methanol. The gradient was: 0 min
948 (3% methanol), 7 min (3% methanol), 32 min (50% methanol), 35 min (50% methanol), 41
949 min (3% methanol), and 45 min (3% methanol). Adenine nucleotides were detected as
950 described above. Separate fractions of roughly 500 µL were manually collected for 2'-deoxy-
951 ADPR (R_t 10.85 min) and 2'-deoxy-NAD (R_t 17.2 min) around the retention times of the
952 respective standards. Fractions were dried on a SpeedVac evaporator and submitted to
953 HRMS. Quantification using external standards was done as described above. Recovery was
954 determined from the internal standard 1, N^6 -ethenoadenosine. Since recovery was always
955 around 100% results were not corrected during these experiments.

956 *High resolution mass spectrometry(HRMS)*

957 HRMS was carried out using ultrahigh resolution ESI-QTOF on a maXis HD Bruker
958 Daltonics instrument in negative mode with direct injection (50 µL). Spectra were acquired in
959 full scan mode in the mass range 100 – 750 m/z and the baseline subtracted (MilliQ water).

960 *Generation of CD38^{-/-} Jurkat cell line using CRISPR/Cas9*

961 Knock-out of CD38 in Jurkat subclone JMP was performed by CRISPR/Cas9 using the
962 expression plasmids pX330-Puro-T2A-hCas9 and pCAG-EGxxFP, which were kindly
963 provided by Prof. Dr. Alexander Flügel (Department of Neuroimmunology, University
964 Medical Center Göttingen, Göttingen, Germany). The sgRNA sequence
965 (CCACCGCGAGCACCACGACG) was designed with the GenScript gRNA design tool
966 (<http://www.genscript.com/gRNA-design-tool.html>). The adapted expression plasmids were
967 co-transfected into Jurkat cells by electroporation. EGFP positive cells from the transfection
968 were sorted and individualized by FACS (FACS Sorting Core Unit, University Medical

969 Centre Hamburg-Eppendorf, Germany). Resulting Jurkat clones were characterized regarding
970 CD38 protein expression and NAD glycohydrolase activity.

971 *Preparation of membrane fractions from Jurkat cells*

972 Membrane fractions from Jurkat cells were prepared as described previously^{50,51}. Briefly,
973 either 5×10^7 wild type Jurkat cells or CD38^{-/-} Jurkat cells were suspended in lysis buffer
974 (110 mmol/L NaCl, 20 mmol/L HEPES, pH 7.4) with protease inhibitor mix (Roche) and
975 disrupted using a dounce homogenizer. After removal of undisrupted cells and intact nuclei,
976 membranes were enriched by centrifugation at 10 000xg. The membrane pellet was
977 resuspended in lysis buffer and protein content determined by Bradford protein assay (Bio-
978 Rad) against BSA as standard.

979 *Assay of NAD glycohydrolase activity*

980 NAD glycohydrolase activity in P10 membranes from wild type Jurkat cells or CD38^{-/-} Jurkat
981 cells was determined as described previously^{50,51}. Briefly, 20 μ g of P10 membrane proteins
982 from wild type Jurkat cells or CD38^{-/-} Jurkat cells were incubated with 1, N⁶-etheno-NAD
983 (100 μ mol/L) in buffer (140 mmol/L, NaCl, 5 mmol/L KCl, 1 mmol/L MgSO₄, 1 mmol/L
984 CaCl₂, 1 mmol/L NaH₂PO₄, 5.5 mmol/L D-glucose and 20 mmol/L HEPES, pH 7.4). In the
985 course of the reaction fluorescence is increasing due to the higher fluorescence of the product
986 1, N⁶-etheno-ADPR compared to the substrate. The increase in fluorescence was followed
987 (excitation at 300 nm, emission at 410 nm) using an Infinite M200 micro plate reader (Tecan).
988 The amount of product formed was calculated from the fluorescence readings using a 1, N⁶-
989 etheno-ADPR standard curve.

990 *Western Blot analysis of CD38 activity*

991 CD38 expression in Jurkat cells was analyzed as described recently^{50,51}. Briefly 60 μ g of P10
992 membrane proteins from wild type and CD38^{-/-} Jurkat cells were separated on a 12% non-

993 reducing SDS-PAGE (0.4% SDS) and subsequently transferred to a PVDF membrane
994 (Immobilon-FL, Millipore). The membrane was probed with a primary antibody against
995 human CD38 (1:200, mouse monoclonal antibody AT-1, Santa Cruz Biotechnology #sc-7325)
996 and a secondary goat anti-mouse antibody conjugated to horse radish peroxidase (1:10 000,
997 Santa Cruz Biotechnology #sc-2302). Incubation of the membrane in SuperSignal Working
998 Solution (Thermo Fisher Scientific) for 5 min allowed for detection of the secondary antibody
999 by chemiluminescence using an Image Quant LAS4000/LAS3000 (GE Healthcare Life
1000 Sciences).

1001 *Statistical Analysis*

1002 Statistical analysis was performed using GraphPad Prism (v 6.03, GraphPad Software).
1003 Quantitative data were tested for normality using D'Agostino-Pearson Omnibus Test
1004 ($\alpha=0.05$). If all groups were normally distributed, data is reported as mean \pm SEM (standard
1005 error of the mean) and parametric tests were used (unpaired, two-tailed T-test or one-way
1006 ANOVA). In case of non-normal distribution or if the sample size for groups was too small to
1007 test for normality, data is reported as median with interquartile range and non-parametric tests
1008 (Mann-Whitney test, Kruskal-Wallis test) were chosen. If non-normal data were to be
1009 compared against a hypothetical value (especially against 0) a Wilcoxon Signed Rank Test
1010 was used. Post-hoc tests were performed as Holm-Sidak or Dunn's test with p-values
1011 corrected for multiple testing.

1012 Linear and non-linear regression analysis was performed using GraphPad Prism (v 6.03,
1013 GraphPad Software). For fitting of concentration-response curves (Fig. 2) a four parameter
1014 logistic model has been chosen. Conditions were: bottom value constrained to 0 and Hill
1015 coefficient shared between data sets. For the analysis of channel inactivation (Fig. 3e+f) a
1016 histogram of the frequency distribution with a bin width of 5 s was generated and a one phase
1017 exponential decay function fitted to the data by non-linear regression. To test whether

1018 parameters of fit differ between conditions extra-sum-of-squares F tests were used. In case of
1019 the slope conductance (Fig. 3c) data were fitted to a linear equation (without intercept). To
1020 compare the slope conductance between channel variants and agonists the results from the
1021 linear regression (slope \pm SEM) were tested by multiple unpaired, two-tailed T-tests assuming
1022 normal distribution of the residuals and without correction for multiple testing.

1023 An a priori power analysis to determine sample sizes has not been done. For all statistical tests
1024 a significance level α of 0.05 was adopted.

1025

1026 **Methods-only references**

- 1027 44. Zhang, B. *et al.* 2'-deoxy cyclic adenosine 5'-diphosphate ribose derivatives:
1028 importance of the 2'-hydroxyl motif for the antagonistic activity of 8-substituted
1029 cADPR derivatives. *J. Med. Chem.* **51**, 1623–36 (2008).
- 1030 45. Kirchberger, T. *et al.* 8-Bromo-cyclic inosine diphosphoribose: towards a selective
1031 cyclic ADP-ribose agonist. *Biochem. J.* **422**, 139–149 (2009).
- 1032 46. Partida-Sanchez, S. *et al.* Chemotaxis of mouse bone marrow neutrophils and dendritic
1033 cells is controlled by adp-ribose, the major product generated by the CD38 enzyme
1034 reaction. *J. Immunol.* **179**, 7827–7839 (2007).
- 1035 47. He, B. & Soderlund, D. M. Human embryonic kidney (HEK293) cells express
1036 endogenous voltage-gated sodium currents and Na v 1.7 sodium channels. *Neurosci.*
1037 *Lett.* **469**, 268–72 (2010).
- 1038 48. Gagné, J. P. *et al.* Quantitative proteomics profiling of the poly(ADP-ribose)-related
1039 response to genotoxic stress. *Nucleic Acids Res.* **40**, 7788–7805 (2012).
- 1040 49. Bobalova, J., Bobal, P. & Mutafova-Yambolieva, V. N. High-performance liquid
1041 chromatographic technique for detection of a fluorescent analogue of ADP-ribose in
1042 isolated blood vessel preparations. *Anal. Biochem.* **305**, 269–276 (2002).
- 1043 50. Schmid, F., Fliegert, R., Westphal, T., Bauche, A. & Guse, A. H. Nicotinic Acid
1044 Adenine Dinucleotide Phosphate (NAADP) degradation by alkaline phosphatase. *J.*
1045 *Biol. Chem.* **287**, 32525–32534 (2012).
- 1046 51. Schmid, F., Bruhn, S., Weber, K., Mittrücker, H. W. & Guse, A. H. CD38: A NAADP
1047 degrading enzyme. *FEBS Lett.* **585**, 3544–3548 (2011).

1048

1049 **Statement on image integrity**

1050 The authors confirm that the paper complies with Nature Publishing policy concerning image
1051 integrity.

1052 **Statement on competing financial interests**

1053 The authors declare that they do not have any competing financial interests.

1054 **Code Availability**

1055 Codes can be obtained upon request from the corresponding author (guse@uke.de).

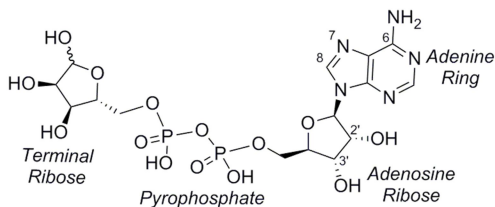
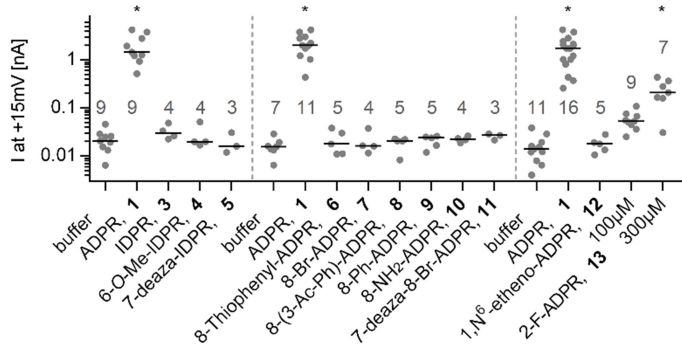
1056 **Data Availability Statement**

1057 Any materials, associated protocols, and other supporting data may be obtained from the
1058 corresponding author (guse@uke.de).

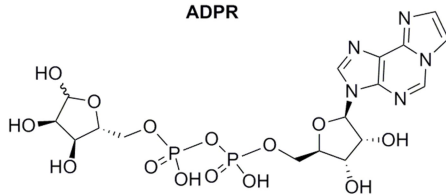
1059

1060

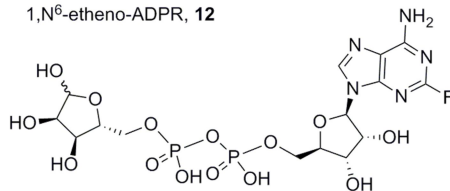
a Adenine Modifications



ADPR

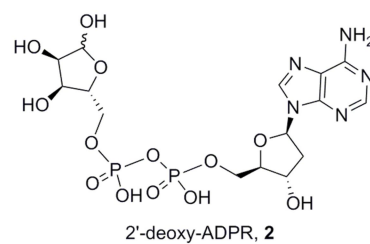
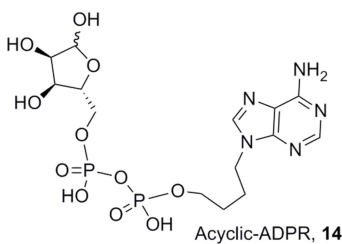
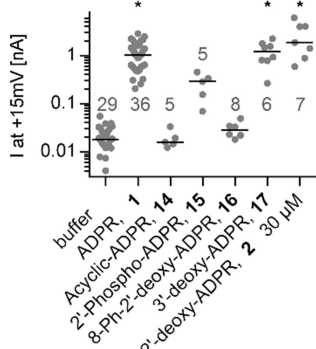


1,N⁶-etheno-ADPR, 12

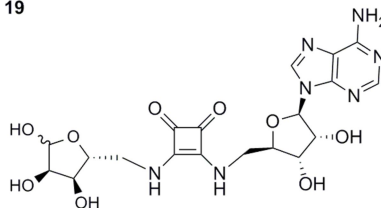
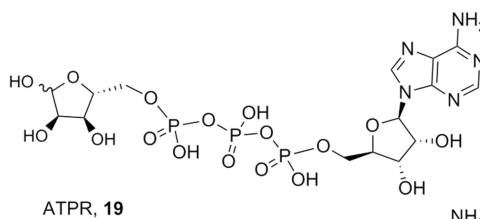
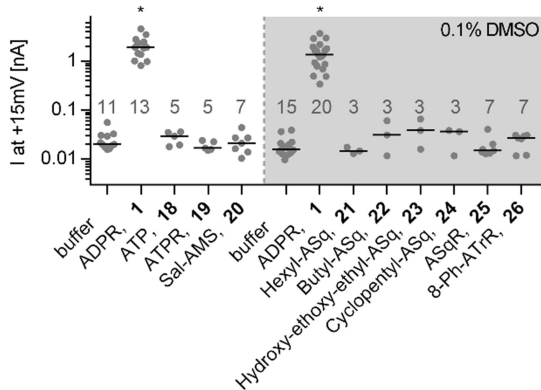


2-F-ADPR, 13

b Adenosine Ribose Modifications



c Pyrophosphate Modifications



d Terminal Ribose Modifications

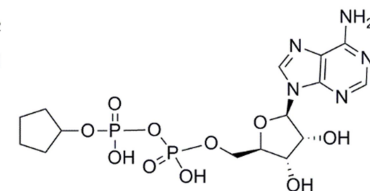
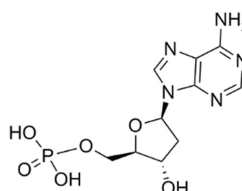
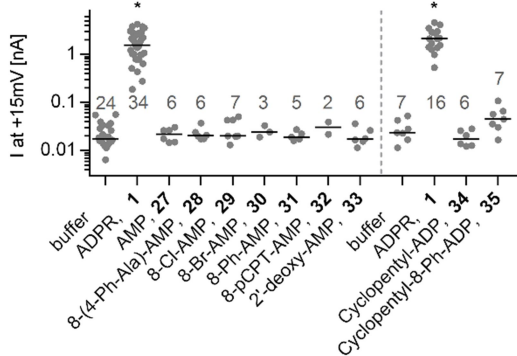
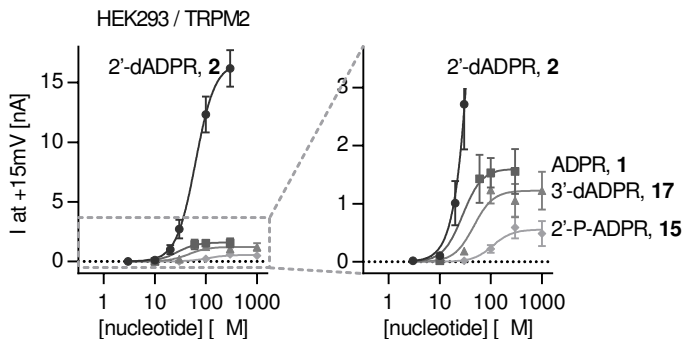
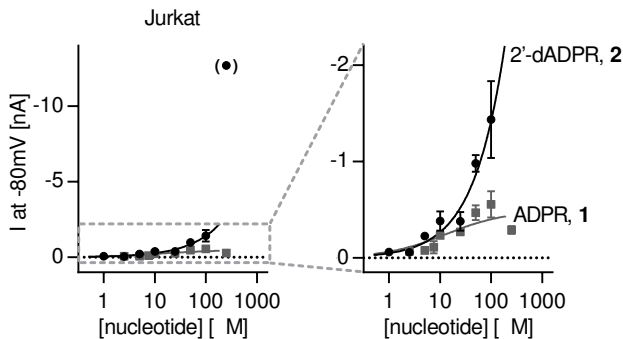


Figure 2

a



b



c

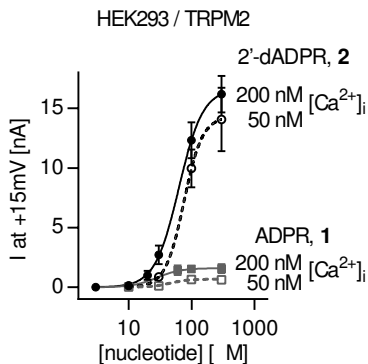


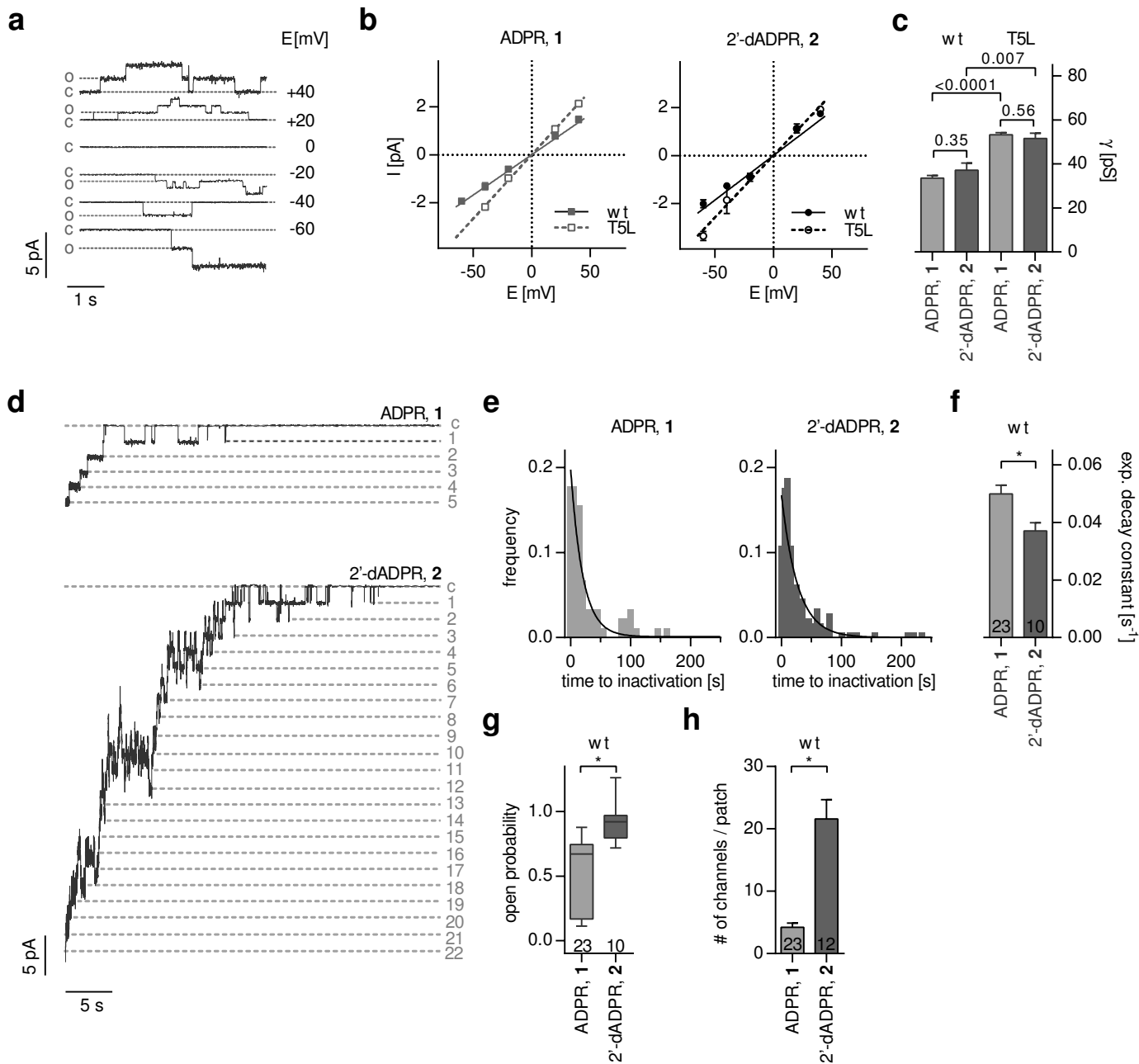
Figure 3

Figure 4

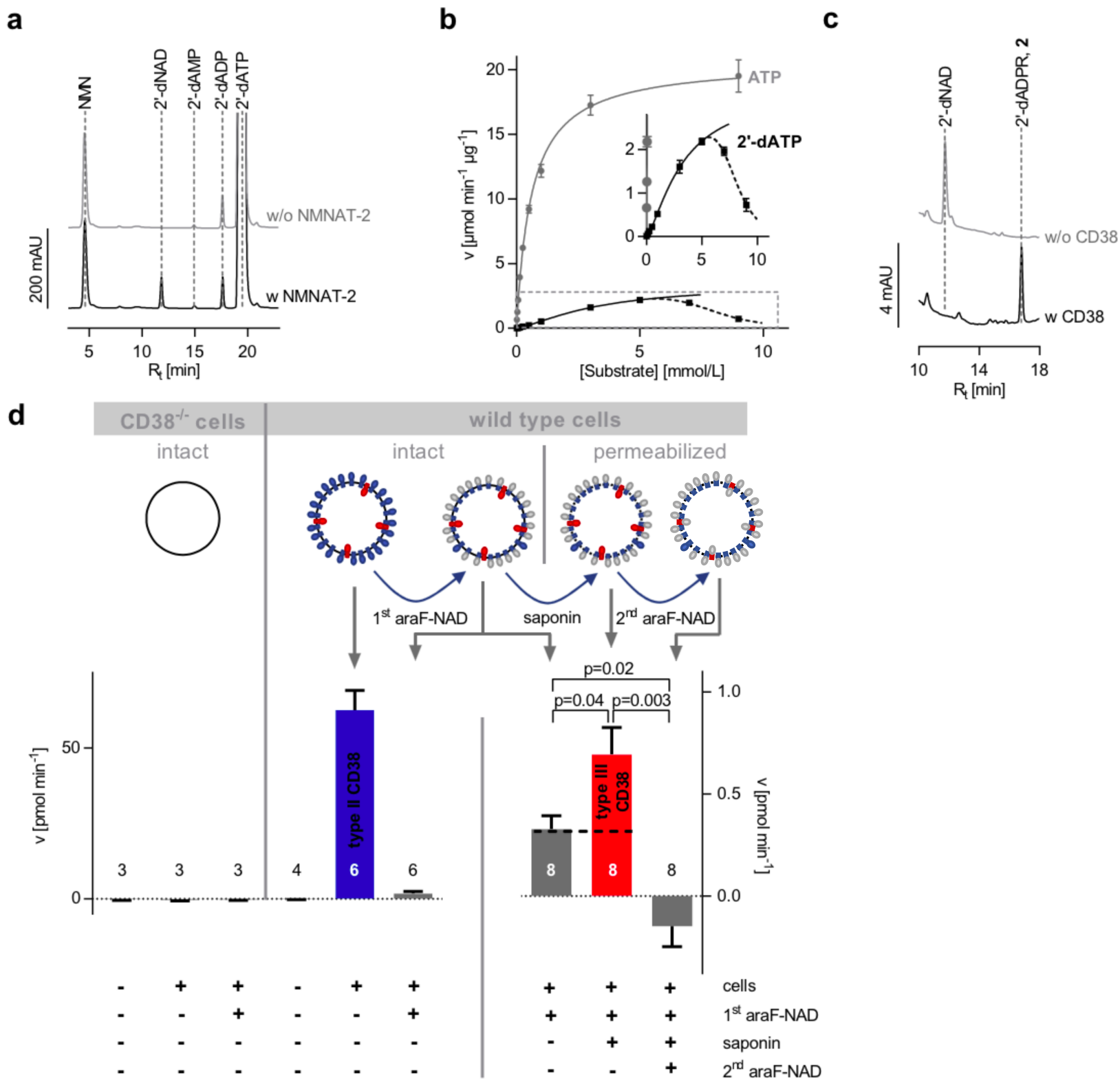


Figure 5

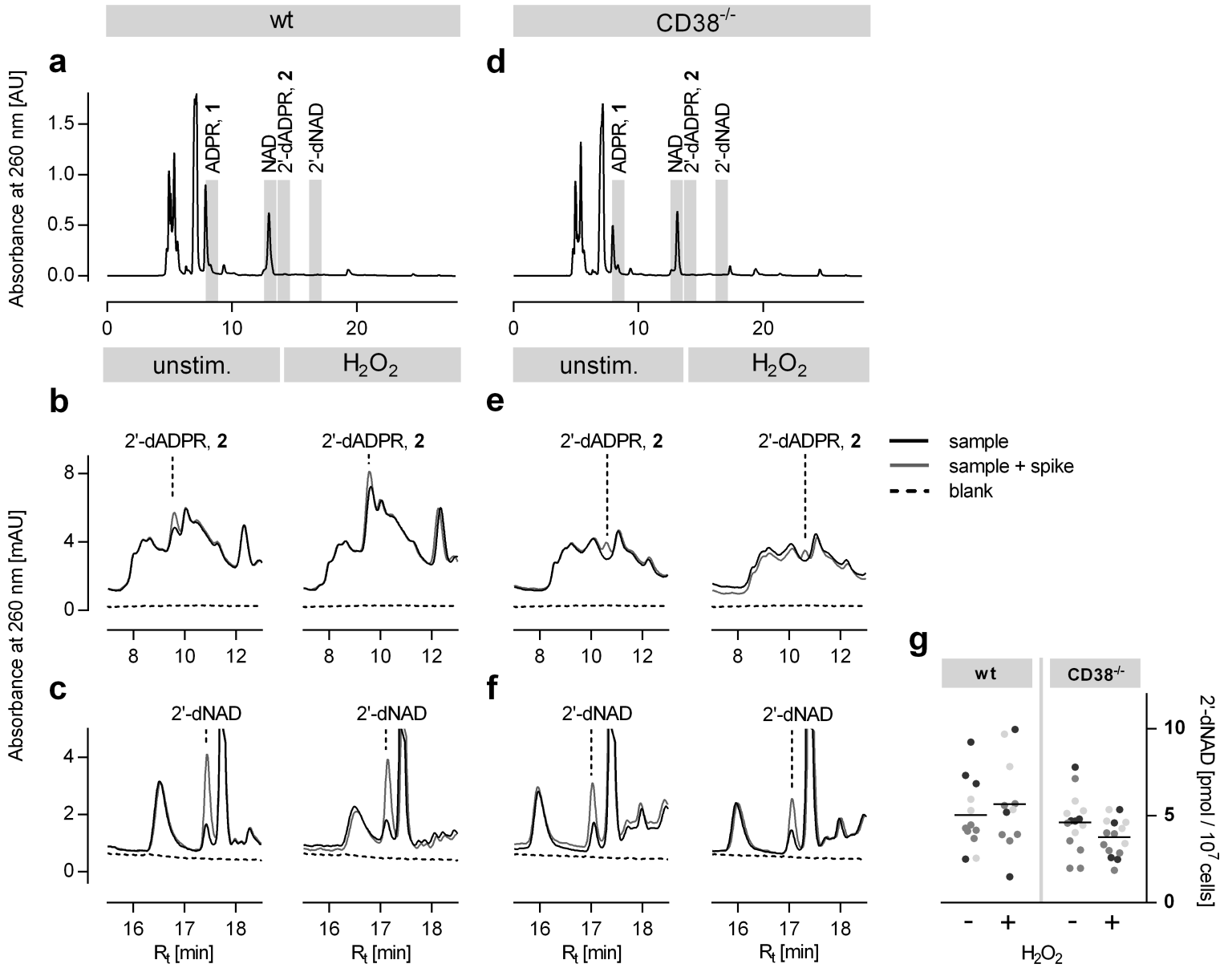
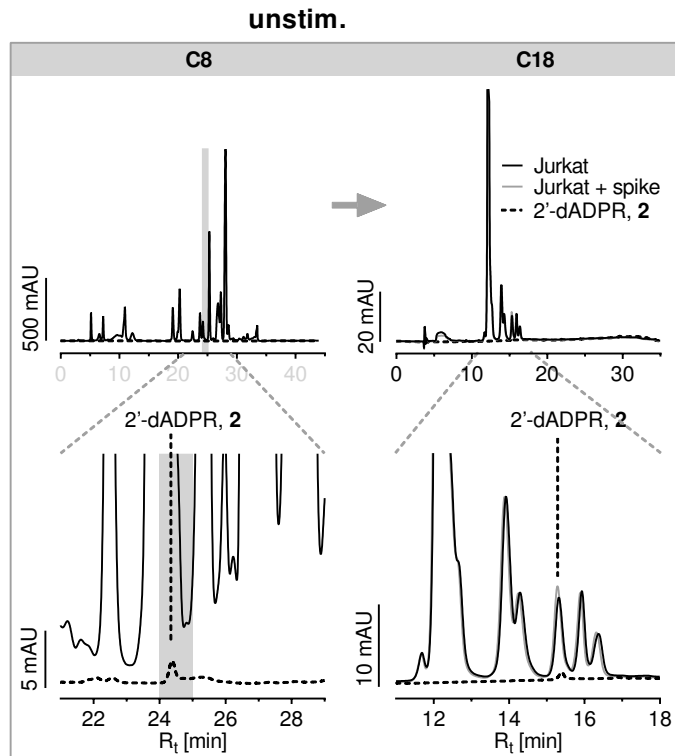
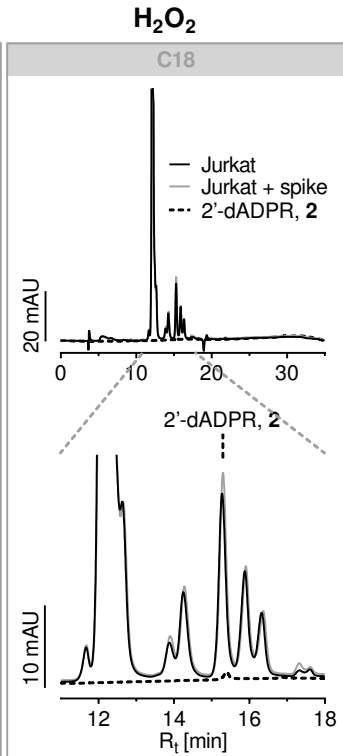


Figure 6**a****b****c**